DURUPT Lauréline

Master Nanotech 2018-2019

MIRSENSE

Centre d'intégration NanoINNOV
Bâtiment 863
8 avenue de la Vauve
F-91120 Palaiseau

Characterization of Quantum Cascade Detector illuminated by a Quantum Cascade Laser

from 04/03/19 to 30/08/19

Confidentiality: no

Under the supervision of:

- **Company supervisor : MAISONS Gregory, gregory.maisons@mirsense.com**
  Present at the defense: no

- **Phelma Tutor : BROQUIN Jean-Emmanuel, broquin@minatec.grenoble-inp.fr**

Résumé:

Les détecteurs infrarouges ont depuis plusieurs années suscité l'intérêt des chercheurs au même titre que les industrielles au vue de leurs bénéfices dans de nombreux secteurs (militaire, environnemental, médical). Dans le but de commercialiser des capteurs de gaz, miniatures et basés sur la technologie des structures à cascade quantique, Mirsense souhaite aujourd'hui étudier la possibilité d'intégrer dans ses analyseurs de gaz un système composé de leur source infrarouge, de type laser à cascade quantique, un gaz à analyser et un détecteur à cascade quantique. Pour certaines applications ce dernier serait susceptible de remplacer la détection acoustique, comme par exemple la communication en espace libre, pour laquelle elle ne peut être utilisée.

Ce stage a donc été l'objet de l'étude de deux échantillons de QCDs à deux longueurs d'onde différentes: 5 µm et 8 µm. Différentes mesures de caractérisation ont été effectué sur ces deux échantillons : mesures courant-tension, mesures de résistance, mesures de leur réponse en fonction de la longueur d'onde, détermination de la détectivité, à l'aide d'un oscilloscope ou d'un FTIR. Malgré une réponse très faible qui risque de compromettre leur utilisation, nous avons pu effectuer des mesures à température ambiante avec ces détecteurs et les utiliser avec l'électronique MultiSense développé par MirSense permettant le traitement du signal détecté. Enfin j'ai pu réaliser dans le laboratoire III-V Lab, des mesures de bruits grâce à l'utilisation d'un analyseur de spectre. Il est délicat d'avoir un avis critique sur ces résultats ; la plupart des articles scientifiques qui traitent des sources de bruit dans les QCDs ne mentionnent pas de valeurs pratiques. Cependant, par extrapolation, on peut affirmer que le niveau de bruit dans un QCD est plus ou moins comparable à celui du QWIP à température ambiante.

Afin de vérifier leur potentiel en matière de détection de gaz, j'ai mis en place un banc optique permettant la spectroscopie de l'eau présente dans l'air ambiant. Une étude préliminaire et théorique m'a permis de dimensionner mon expérience pour des distances d'absorption trop courtes. J'ai donc créé une cellule d'Herriott dans le but d'augmenter le chemin optique, et les résultats d'abord effectués avec un détecteur MCT ont été concluants puisque le pic d'absorption de l'eau était bien visible. Malheureusement, les QCDs quant à eux, n'ont pas permis cette observation du fait de leur faible réponse. L'utilisation d'un amplificateur de courant s'est donc présentée comme nécessaire et nous avons finalement pu observer le pic d'absorption de l'eau.

Abstract:

For several years now, infrared detectors have always sparked the interest of researchers as well as industries in view of their profits in many areas (military, environmental, medical). In order to commercialize smaller gas sensors based on the technology of quantum cascade structures, MirSense wants to look into an integrated system composed of its infrared source which is a quantum cascade laser, a gas to detect and a quantum cascade detector. For any application, such as free space communications, the latter would replace the acoustic detection already present in module for sale.

This internship was about the study of two QCDs' samples at two different wavelengths: 5µm and 8µm. Various characterization's measures were done on these two samples: current-voltage measures, resistances measures, QCDs' response depending on the wavelength, detectivity measurement, using an oscilloscope or a FTIR. Even if these detectors are tarnish by a very weak response that could adversely affect their use, measures at room temperature with these detectors were performed and we were able to use them with the MultiSense electronics developed by MirSense to process the detected signal. Lastly, noise measurements were carried out in III-V Lab, using a spectrum analyser. However it is quite delicate to be critical of the results obtained. Indeed most of scientific papers deal with noise sources in QCDs without giving orders of magnitude. Then I had to extrapolate results from QWIP experiments in order to draw a comparison with my results. I can conclude that noise QCDs values are more or less identical to QWIPs at room temperature.

In order to check their potential for gas detection, I set up an optical bench for spectroscopy of water present in the air. A preliminary theoretical allowed me to size my experience for too short distances of absorption. So I created a Herriott cell in order to increase the optical path, using at first an MCT detector. The results were conclusive since the water absorption line was clearly visible. Unfortunately when using QCDs, the absorption line was not any more visible due to the weak QCD's response. We had to add a current amplifier which allowed us to observe the water absorption line.

Presentation of MirSense:

MirSense is a French start up created in 2015 which was at the beginning hosted by Thales facilities. They are developing and manufacturing optoelectronic devices:

- A single gas laser which is a tunable mid infrared source for gases spectroscopy;
- A multi-gas laser module which is a mid-infrared spectrometer all-inclusive.

The advantages of such technologies consist in being compact and smaller in size since they substitute a wide variety of optical components to achieve the same tasks.

MirSense settles in different markets such as:

- Environment and pollution monitoring thanks to their spectroscopy module for gas sensing;
- Biology and health care with application such as glucose monitoring, breath analysis;
- Military and defence to counter rockets thanks to directional infrared measure.

Their technology is based on the quantum cascade laser which emits light in the mid infrared (from 4 to 12 µm) up to the terahertz domain and operate either in pulse regimes either in continuous-wave regime at room temperature. They have developed two types of source:

- Fabry-Perot laser which is multimode laser sources;
- Distributed Feedback laser which is single mode laser sources.

Nowadays, they are using photoacoustic detection for their MultiSense sensors. This phenomenon is attractive since we can reach sensitivity of the order of one ppm while remaining with a compact device. However some environment are not suitable for photoacoustic detection (for example if you are trying to detect over a long distance) and therefore MirSense wants to integrate quantum cascade detection in their sensors.

Acknowledgment:

I express my deepest gratitude to Gregory Maisons, my supervisor, who took time to guide me during my internship even though he was busy with his works. Thank you for your kindness and your precious advices.

Thank you to my Phelma's Colleagues Timothée Lassiaz and Maxime Guais without whom I probably would not have known MirSense.

Thank you to Mathieu Carras, CEO of MirSense, for accepting my application to be part of the company for these six months, as well as for the interesting discussions we had regarding my results.

A special mention for Ali Fortas who took time to explain me how work the drilling machine, other mechanical tools and who give me precious experimental tips.

I was very lucky to work with all my kind colleagues, and I am very excited to come back in MirSense to start my PhD with all of you.

Glossary:

- QCD : Quantum Cascade Detector
- QCL : Quantum Cascade Laser
- QWIP : Quantum Well Infrared Photodetector
- MCT : Detector based on Mercury-Cadmium telluride
- TIA : Trans Impedance amplifier
- FTIR : Fourier Transform InfraRed spectroscopy
- SEM : Scanning Electron Microscopy

List of figures:

Mathematical notations:

- $c = 2.99792458 * 10^{8}\ [m/s]$ Speed of light
- $q = 1.60217662 * 10^{-19}\ [C]$ Elementary charge
- $h = 6.62607004 * 10^{-34}\ [J.s]$ Planck's constant
- $k_B = 1.38064852 * 10^{-23}\ [J/K]$ Boltzmann's constant
- γ Hooge's constant

Gantt Diagram:

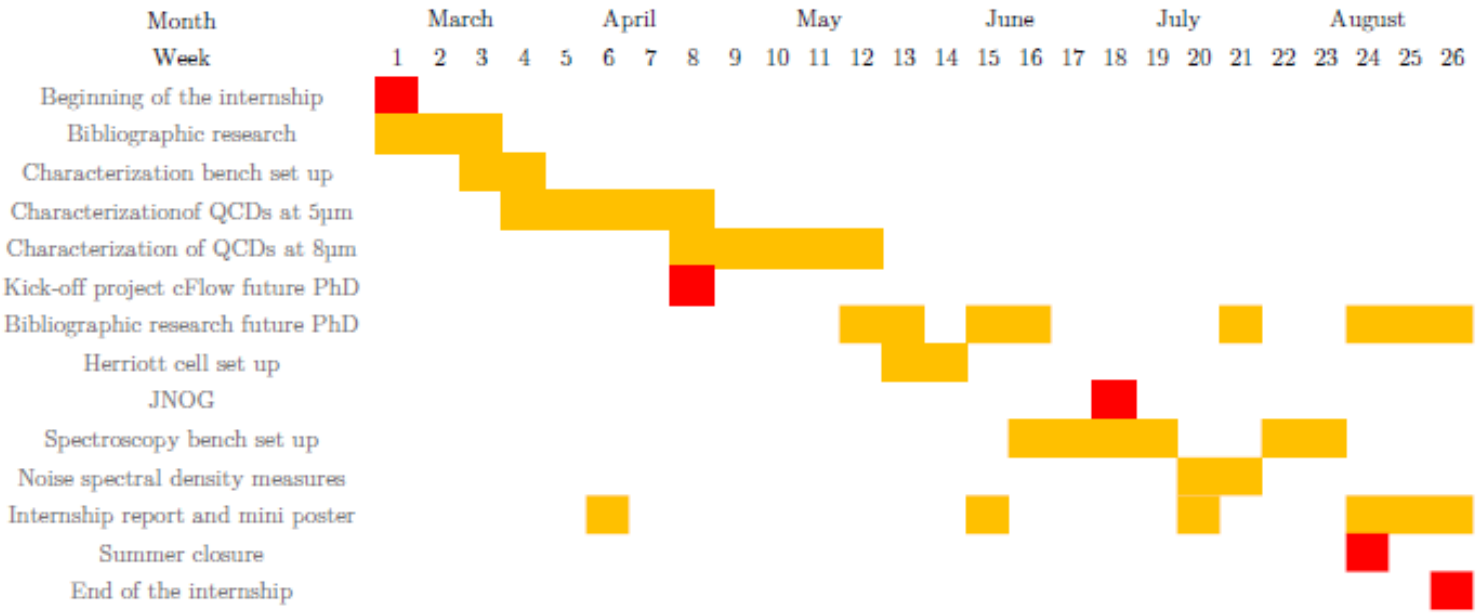

Cost Evaluation of the internship:

	Cost
Administrative	
Internship remuneration	6 000,00 €
JNOG inscription	200,00 €
Purchase order	
Mounting	54,00 €
Red laser	80,00 €
Breadboard	305,00 €
Electronic	38,00 €
Mechanic	18,00 €
TOTAL	6 695,00 €

Table of contents:

Introduction:

The 20^{e} century was marked by impressive advances in micro and nanotechnology which today compose the majority of electronic devices.

Let's take a camera as an example. This state of the art which has been sold worldwide allows for their user to detect visible light thanks to a sensor. For several years, areas such as military field as well as environment, found an interest in using a camera for infrared detection. Thanks to the development of epitaxial growth, quantum cascade heterostructures whose principle is based on interbande transitions, are the best candidate for these applications. Their structure composed of a stack of two semiconductors allows to adjust detector's features by playing with the scaling of the different layer.

Currently Mirsense gas analysers take advantage of acoustic cells for sensing. The 21e century allows for the emergence of a new kind of detector: quantum cascade detector (QCD). Their technology combines two kinds of heterostructure devices: the Quantum Wells Infrared Photodetector (QWIP) and the Quantum Cascade Laser (QCL). Mirsense's ambition is to develop an integrated chip which includes a QCL and a QCD for infrared spectroscopy. Such a system requires an identical technology for both emitter and detector, and thus bans all other types of detectors.

During this internship I tried to respond to two specific objectives: The first one is the study of QCDs and more specifically their behaviour when they are illuminated by QCL. The second one is to integrate the QCD in a spectroscopic system by setting up an optical bench for gas detection.

This work is divided in two parts. First the knowledge essential to the understanding of the operation of QCDs is underscored as well as their stakes and their place in the industrial world. Then my experimental work is highlighted in the second chapter. It includes characterisation measurements of two samples: ART3040-7 and T364-7 which are QCDs sensitive to wavelength at 5µm and 8µm respectively. An infrared spectroscopy of water absorption line is also carried out at the end of this part.

Chapter I:

Introduction to infrared quantum detection

This section establishes the application context and theoretical knowledge used to understand the quantum cascade detector operation as well as the different figures of Merit and main parameter that characterize their performances.

I.1. Infrared imaging

I.1.a. Interest in infrared imaging

Infrared is the wavelength range 0.76µm - 1000 µm. For several years, a subdomain to the infrared area interest especially researchers: the mid-infrared which cover a wavelength from 2 µm to 20 µm approximately. Two atmospheric windows, the first one between 3 µm and 5 µm and the second one between 8 µm and 14 µm, are interesting for industrial applications.

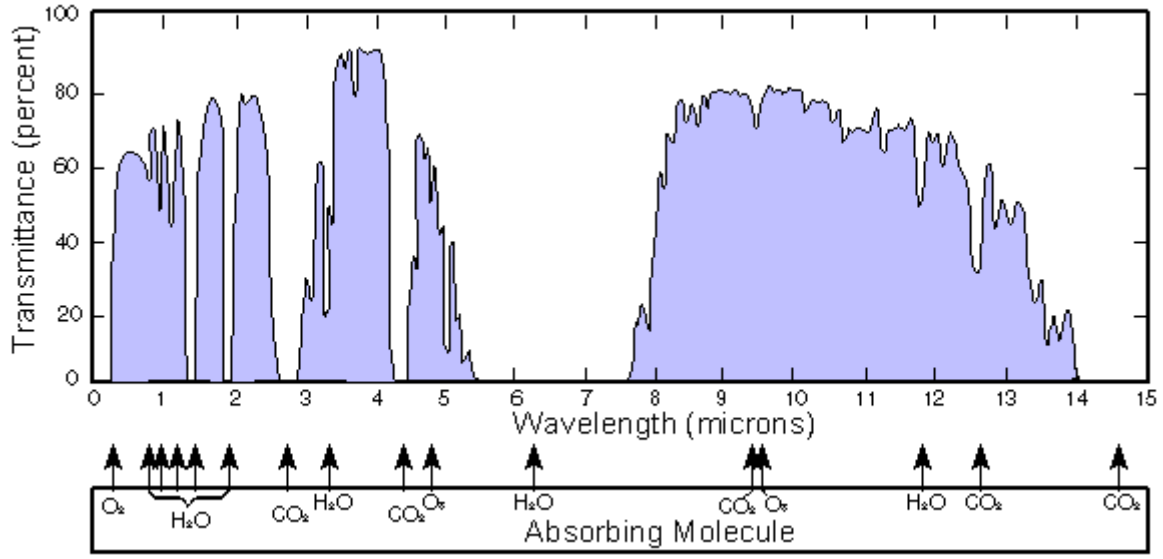

Figure 1: Atmospheric transmittance in the mid infrared region.[2]

Contrary to visible range for which a body is brought to reflect ambient radiation, each body represent an infrared radiation source which have a major impact upward 3 µm. Henceforth we can find an interest in working at infrared wavelength for night vision or even thermal imaging.

Most of gas molecules own resonance in the mid infrared wavelength range and can be excited by these energies. As a result, the surrounding radiation is absorbed by the gas molecules. The absorption amplitude is directly linked to the quantity of these specific molecules. From this, spectroscopy measurements can be carried out in order to probe the gas composition of the environment and allow, as an example, to detect drugs, pollutant, explosive, as well as the quantity of glucose in blood.

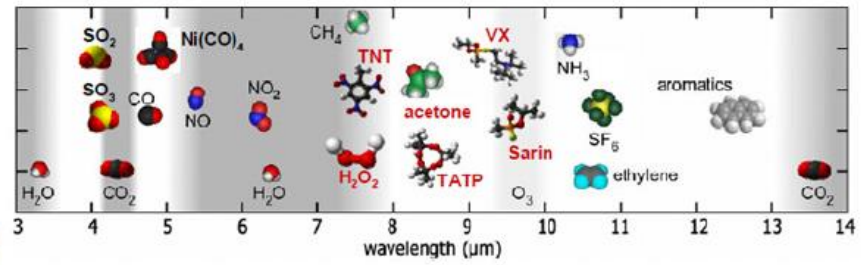

Figure 2: Molecules which are possible to detect in mid infrared region. [6]

At last, another relevant application is based on the transport of information at high bit rate and in particular free space optical communication. A laser signal is modulated and propagates through the atmosphere where it is collected and processed in order to extract information. From this, a network composed of a couple source/detector spread in the heart of a city can be imagined to ease information sharing.

MirSense is currently using acoustic detection [16]: gas molecules are excited by the QCL beam of frequency υ, provided that hυ correspond to an energy transition for the gas specie. Then molecules can go back to their fundamental state, dissipating their absorbed energy by collision with neighbouring molecules. The resulting local heating gives rise to a pressure wave which is detected by a microphone. However this detection required to have the source and the detector close to each other. Therefore some application such as free space communication cannot be envisaged. For this reason, MirSense is trying to find an alternative to the photoacoustic detection, using a quantum detector for which the distance between source and detector can handle several kilometres.

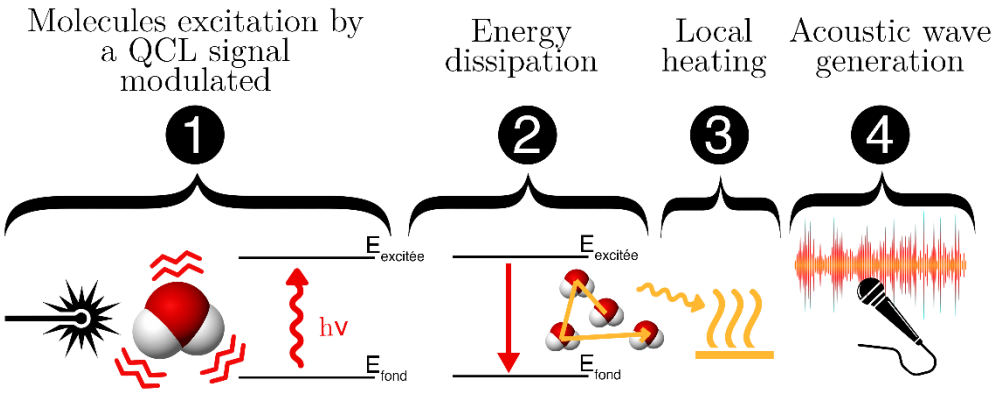

Figure 3: Principle of photoacoustic detection.

I.1.b. Type of detectors

I.1.b.i. Thermal detector

Thermal detectors cover thermopiles, bolometers, pyroelectric detectors. They are the first detectors developed and commercialized. Their principle is based on fluctuation of a physical property (resistance, voltage…) due to the absorption of incident radiation and consequently heating of the detector. They are able to detect a wide wavelength range at room temperature which face significant demands on the infrared camera market. However they are tainted by a slow time response (higher than tens of millisecond). Moreover they need to be thermally insulated from room environment and are not selective. Circa 1935, researchers looked into a new technology in order to counter these problems: quantum detectors.

I.1.b.ii. Quantum detectors

Quantum detectors are very sensitive and are based on electronic transitions between energy levels follow-up to photon absorption. They are two types of quantum detection:

- Inter-band detection: detectors are made from MCT and are based on the absorption of a photon whose energy hυ is higher than the gap energy which excite an electrons from the valence band toward the conduction band. Then photocurrent is collected by simply separating the electron-hole pair by an electric field. However this type of transition is not achieved correctly in the mid infrared field.
- Intra-band detection: electrons may either cross a potential barrier due to the absorption of a photon (Schottky photodiode), either flow from one energy sub-band to another within the conduction band. These sub-band are created by quantum well structure. The main advantage of this kind of detector consists in the possibility of adjusting the wavelength of detection by playing with the materials used and the sizing of these quantum wells. Afterward, these detectors will be of interest.

Unfortunately they have to be maintained at a low temperature because of thermal agitation which disturb transitions between energy level: the larger the wavelength, the lower the temperature is required.

I.2. Types of quantum well infrared detectors

I.2.a. Single quantum well detectors[1]

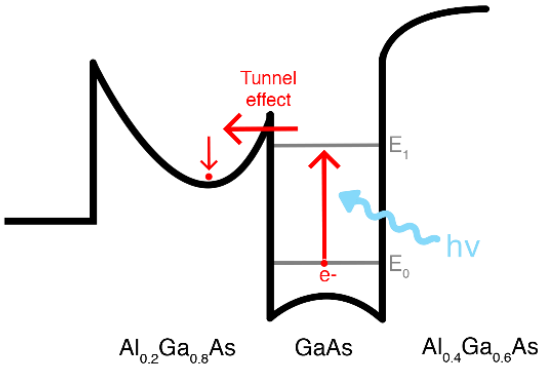

Figure 4: Schematic profile of the conduction band of a single quantum well detector.

One example of basic quantum well detector conceivable is a single well detector composed of a GaAs layer sandwiched between two AlGaAs layers with a different doping. By doping strongly one of the AlGaAs layer, the conduction band is bending, a parabolic potential well is therefore obtained and allows for carriers displacement. A photon with a sufficient energy provides the excitation needed for an electron to pass from the fundamental level E_0 to an excited level E_1. The electron can tunnel from the square well to the parabolic well since the barrier is thin. Then it relaxes in the parabolic well at the lowest energy state. To adjust the detection wavelength, the width of the square well has to be adapted: the thinner the well, the higher the energy level E_1, the smaller the wavelength, and the easier will be the delocalisation of the electron. However this model cannot be used in experimental because of an efficiency far too low.

From this simple model, two technologies have been carefully designed and sold on the market: quantum well infrared photodetectors and quantum cascade detector.

I.2.b. Quantum Well Infrared Photodetectors (QWIP)

A QWIP structure is organized in a succession of periods each composed of a thin layer of low gap material GaAs, surrounded on both sides by a larger gap material AlGaAs, in order to achieve a potential well. On each side of the structure, GaAs silicon doped layers are used to inject electrons.

The structure has to be polarized so that electrons can flow in the external circuit and thus record the signal from a source. Under illumination, photon absorption ensures

the transition of an electron from the fundamental level to the excited level of the quantum well. An electric field sweep away photoelectrons out of the well [2]:

- By bound-free transition from the excited level of the continuum without having to cross by the tunnel effect. Electrons are then collected efficiently without applying a strong polarization voltage.
- By bound-bound transition from the excited level to the continuum by tunnelling effect which allows a strong absorption.
- By bound-nearly bound for which the excited level is in resonance with the potential barrier and allows to combine the two advantages of previous transitions as well as a reduction of dark current. It corresponds to the current supplied by the detector without illumination. It comes from different phenomena such as thermal excitation which free charge carriers or the ambient thermal radiation. This last usually leads to a rapid saturation of the capacity included in the readout circuit responsible for collecting information from the detector.

Unfortunately, dark current in these devices remains still crucial and required to cool down the detector to approximately 80K which make its integration with the source difficult. However by being rid of bias voltage, dark current can be drastically reduced, and this can be achieved by quantum cascade detectors.

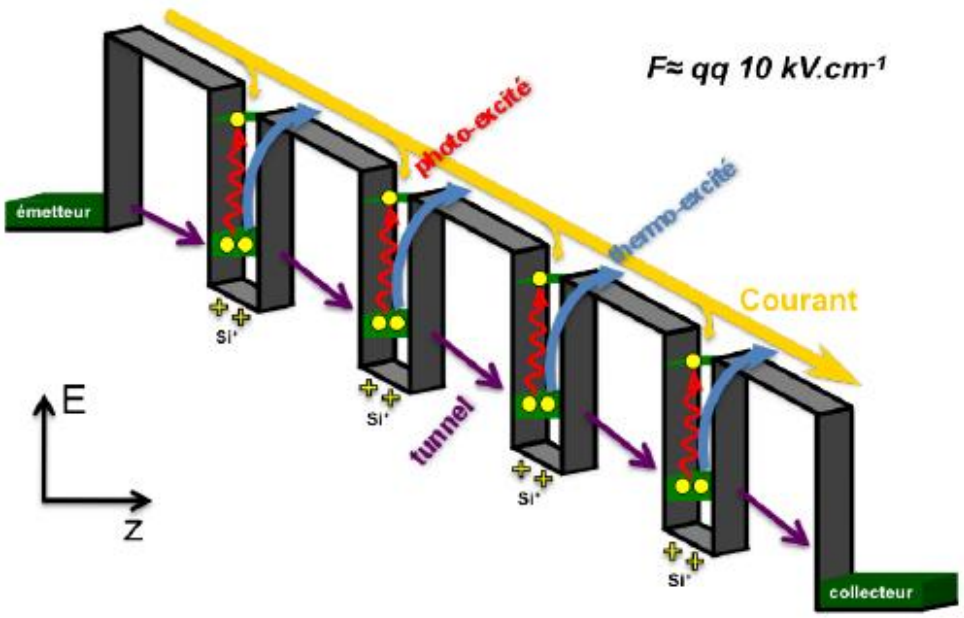

Figure 5: Schematic profile of the conduction band of a QWIP. [8]

I.2.c. Quantum Cascade Detectors (QCD)[3]

I.2.c.i. Structure et principle of detection

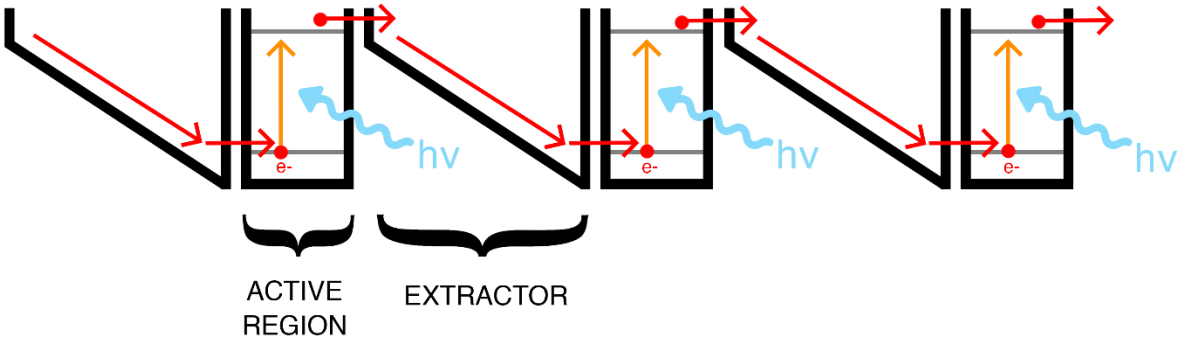

Figure 6: Schematic profile of conduction band of a QCD.

QCD is defined by a multitude of periods each consisting of an active well doped which is the active region dedicated to absorption, and an extractor which is a cascade of several undoped wells to optimize the electron transfer from one period to another.

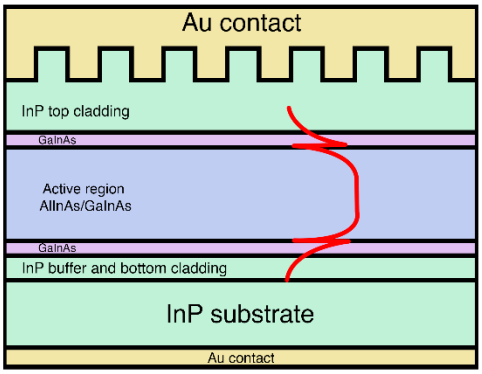

Figure 7: Schematic structure of a QCD.

The advantage of such a structure is to introduce an asymmetry of the potential to allow the electrons photo-excited to escape in a specific direction and then to produce a photo-current. The absorption of a photon of suitable wavelength excites an electron from the fundamental level to an excited level E_2. The transfer of this electron toward weaker energy levels of the next wells is assisted by longitudinal optical phonons emission. Then the photoelectron enters the first well of the following period, identical to the well where it has left. Consequently, no bias is expected to collect a photo-current.

Figure 6 shows the structure and materials of the QCDs that we are using in our experiments. It is answering to specific objectives:

- InAs and GaAs have the same crystalline structure, Blende type, a lattice parameter very close one from the other and a gap energy quite different. Thus it is possible to mix InAs and GaAs in order to obtain a new component $In_xGa_{1-x}As$

(0<x<1) with an energy difference between first levels of the conduction band varying between the one of GaAs and InAs. The choice of $In_xAl_{1-x}As$ is explained by the same argument with the couple InAs/AlAs. At the end, using these new components, it is easy to tune the active region by choosing the In concentration x.

- GaInAs layers on each side of the active region: make the mode more homogenous inside the active layer;
- InP cladding layers: avoid optical losses in highly doped layers;
- Grating at the interface metal-InP: absorbed incoming light.

Several parameters such as the number of periods and the doping have a great influence on the response and noise of the detector. In this report no information about these parameters will be given because of their confidentiality.

I.2.c.ii. Electronic transport

By solving the Schrodinger equation for an infinite square well, energy levels can be calculated and are given by:

$$E_n = \frac{h^2 * n^2}{4\pi^2 * 8mL^2} \, , n > 0 \; (1)$$

Where m is the effective masse and L the width of the well.

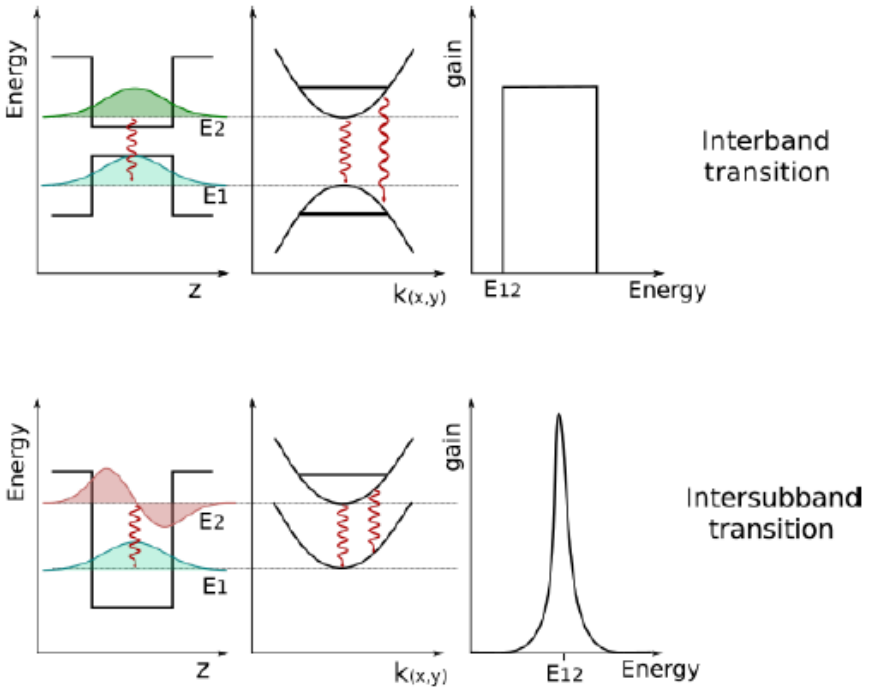

Figure 8: Schematic band diagrams and gain diagrams of interband transition and intersubband transition. [4]

Transitions responsible of electronic transport in the structure are inter-subbands transitions between states of the same band. Electrons located in a level of energy E can absorb a photon of energy hυ in order to find themselves to an excited level of energy E+hυ. Intersubbands are easily adjusted by changing the thickness of the quantum wells. It is a significant advantage compared to interband transitions for which the minimum photon energy absorption or emission is limited by band gap energy. Besides, the energy difference between two subbands is constant and independent of the wave number [4].

From equation (1), the thinner the quantum well the higher the energy level E_n. So extractor can be designed according to the figure 8 by adding several quantum wells of different width, to allow the transfer of the photoelectron from the level 6&7B to the level 1B.

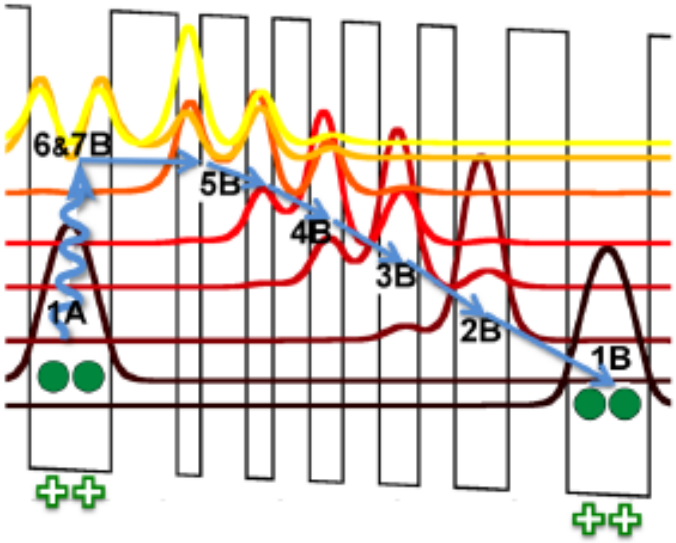

Figure 9: Schematic transfer of photoelectrons from a period to the next. The curves in different colours are the wave functions. [8]

Several physical phenomena are involved when an electron flows from a subbands to the following: spontaneous emission, inelastic diffusion by a phonon, elastic diffusion by impurities or interface defects, as well as electron-electron diffusion [5]. In our case, the phenomenon of optical photon dominates and is responsible for the displacement of the photoelectron, giving a carrier lifetime of the order lower than 1ps. This value is far below 1ns which is the carrier lifetime for interband transitions dominated by electron-hole recombination time. This characteristic leads to one of the major advantage of QCD: this impressively fastness.

I.2.c.iii. Optical coupling by metallic grating[7]

Internal quantum efficiency is defined by:

$$\eta_{int} = \frac{Number\ of\ emitted\ electrons\ by\ the\ wells}{Number\ of\ incoming\ photons}$$

This value is never equal to 1 because of quantum wells are sensitive only to a single polarization: the electric field has to be polarized in the material growth direction, i.e. perpendicular to the layers of the quantum wells. In this way, energy levels are quantified along the axe normal to the layers and free in the other directions so that we have to excite along the quantified axe to have a transition. Thus an optical coupling has to be settle in order to make the incident light absorbed by the active layer and usually a metallic grating etch on the top of QCD fit the bill. However despite this coupling, the absorption in the active layer is rarely equal to 1 because of optical losses in the metal and an emission probability lower than 1.

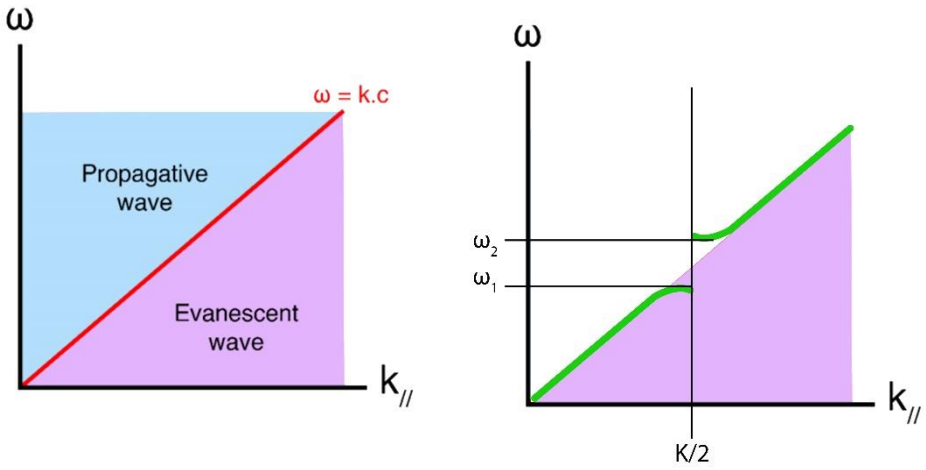

Figure 10: At left: Schematic dispersion curve of a metal-dielectric interface. At right: Schematic representation of a dispersion curve for a grating coupling with opening of the gap.

At the metal-dielectric interface, the dispersion curve is given by:

$$\frac{\omega^2}{c^2} = k^2 = k_{||}^2 + k_{\perp}^2$$

It follows that:

- Above the curve: $\frac{\omega}{c} > k_{||} \leftrightarrow k_{\perp} \in R$ thus the wave is propagating. (Radiative area).

- Below the curve: $\frac{\omega}{c} < k_{||} \leftrightarrow k_{\perp} \in iR$ thus the wave is evanescent and confined at the metal-dielectric interface. Regarding the field, it is perpendicular to the grating and absorbable.

The grating is modifying the dispersion diagram and allows a confinement of the field for three principal reasons: an opening of the forgiven band in the dispersion diagram (dominant for the studied wavelengths), the Plasmon-Polariton resonance and the slot mode excitation (which will not be discussed in this report).

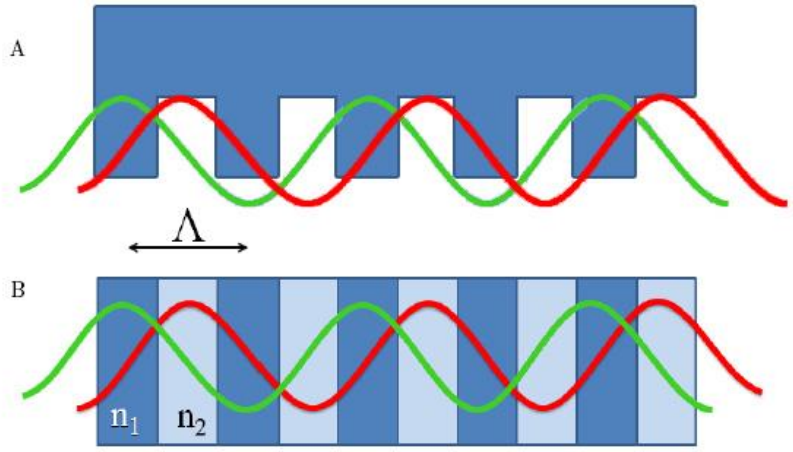

Figure 11: Analogy between stationary states of a Bragg grating (A) and a Bragg mirror (B).

A periodic grating has the same behaviour than a Bragg grating for wavelenght equal to two times the periodicity of the grating Λ. This situation is similar to the Bragg mirror which is composed of a stack of two dielectrics of different indices. The wave propagating meets two different mediums: it does not identically pass through these different materials. Two stationary states can be highlighted: a wave which has its nodes of pulsation ω_1 in the first medium, another with its nodes of pulsation ω_2 in this second medium. We are facing two systems of stationary waves of period 2*Λ. Both modes have their antinodes in different samples and thus do not have the same energy. However, they are described by the same wave vector $\frac{K}{2}$. This wave vector overlaps with the first Brillouin zone. At this location, the breaking of degeneracies forms a photonic bandgap due to the energy difference between these two modes. This gap corresponds to pulsations ω for which the incident wave is reflected. For a strong difference of indices, the gap is becoming larger [6].

The same behaviour is observed in metallic grating: as it is shown in the figure 11 the field is not penetrating in the same way for interstices and bumpers (by the way, the field is nulled for perfect metal). Thus the wave is propagating in two different mediums which induced a gap in the border of the Brillouin area. This phenomenon forces the

lower band under the curve ω = k.c, and therefore allows trapped modes. The band gap in $k = \frac{K}{2}$ allows to obtain a weak confinement for modes in $k = K$. Nevertheless the couple modes, with a wavelength which coincides to the grating's step, are obtained by a second band gap in $k = K$.

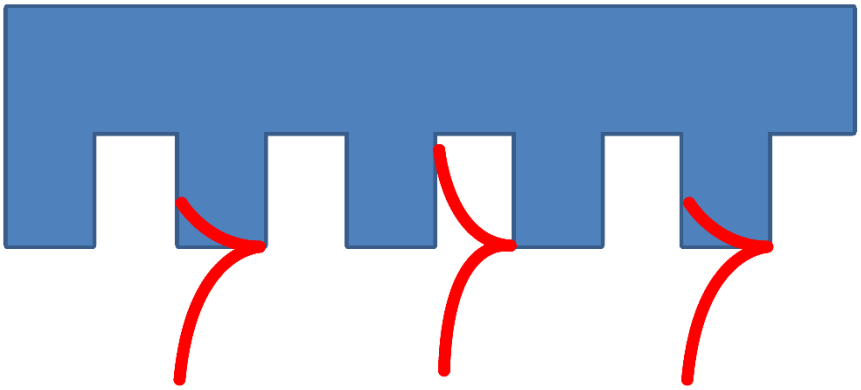

Figure 12: Schematic field profile when a wave is propagating at the metallic grating surface [8].

Another possibility to couple the incident wave to evanescent surface waves comes from surface Plasmon-Polariton. At the Plasmon resonance, electrons are oscillating collectively. The incoming light (photons) is coupled with electrons coming from the metal covering the grating. It is then possible to cause the emergence of a gap within the dispersion diagram for a specific interface with a period adapted to the wavelength of the electromagnetic modes [7].

I.3. Figure of Merite of quantum cascade detectors[8]

I.3.a. Spectral response

- Absorption :

$$\propto = \frac{Number\ of\ absorbed\ photons}{Number\ of\ incoming\ photons}$$

- Emission probability :

$$p_e = \frac{Number\ of\ emitted\ electrons}{Number\ of\ photoexcited\ electrons}$$

- External quantum efficiency :

$$\eta_{ext} = \frac{Number\ of\ electrons\ collected\ at\ the\ contacts}{Number\ of\ incoming\ photons} = \frac{I_S * h\upsilon}{q * P_S}$$

Where I_S is the current produced by the detector and P_S is the optical power. This physical value is significantly affected by recombination phenomena and electron diffusion.

- Spectral response :

$$R = \frac{q \times \lambda \times \eta_{ext}}{h \times c}\ [A.W^{-1}]$$

Where q is the elementary charge, h the Planck constant, c the speed of light in a vacuum and λ the wavelength of incoming photons.

Regarding QCDs, electrical conversion efficiency expressed by $\beta = \frac{\eta_{ext}}{\propto}$ is equal to the reciprocal of the period's number in the structure: an electron passes through the structure conditionally upon there are as many photons as periods.

I.3.b. Noise sources in QCDs

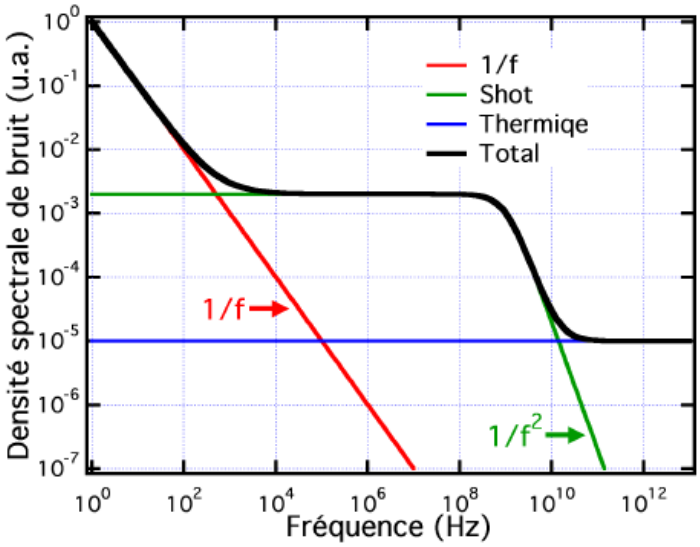

Figure 13: Simulation of the spectral noise density is usually summed up by three contributions: at low frequency 1/f-noise is dominating then shot noise takes over until its cut off frequency. Thermal noise stays constant for any frequency. [8]

Noise induced a random variation of the signal that prevents a precise and correct reading of the detected response which alter the performance of the device.

The first advantage of QCDs lies in its mode of operation at zero bias which allows reducing the dark current and thus use longer integration time without overloading the capacity of the reading circuit. Although QCD is influenced by a noise lower than other quantum detectors, it is still subject to several sources of noise limiting its performance:

- Thermal noise or Johnson noise:

At thermodynamic equilibrium, thermal agitation of charge carriers causes a fluctuation of the measured current at the terminals of the sample and thus induced a noise which is dependent on the temperature T and resistance R of the specimen by the following relationship:

$$S_I = \frac{4k_BT}{R} \; et \; S_V = 4k_BTR$$

Where S is the spectral density of the noise.
For this reason, $R(V = 0V) * Aire$ parameter is often interesting when studying the QCDs.

- Shot noise :

This noise is due to the quantization of physical phenomena, more specifically to the discreet nature of charge carrier whose transport fluctuates randomly and obeys a Poisson's law:

$$S_I = 2q\langle I \rangle$$

Generation-recombination mechanisms are involved to the fluctuation of the number of carriers. This is due to the capture of electrons by a well or the random emission of an electron.

Shot noise current is defined as the sum of two contributions: the dark current and the photon current noise. Indeed, in the infrared range, the photodetector always detect photons coming from their environment which can induce a background limited infrared photodetector phenomenon. This regime is characterized by a thermal noise practically suppressed and only the noise specific to the detector occurs. An unwanted photocurrent due to the surrounding radiation which matches with the limit $I_{obscurité} = I_{photocourant}$ is then appearing.

- 1/f noise :

At low frequency, its effect goes far beyond the shot noise. Discussions around the origin of this noise are contested: some scientists argue that surface effects, including defects trapping and releasing randomly charge carriers, participate in the fluctuation of

the mobility of these last. Other researchers claim that massive effects of the crystal lattice are instead responsible for this noise. However an empirical model seems convinced public opinion and is given by the following expression:

$$S_I = \frac{\gamma I^2}{N\omega}$$

Where γ is the Hooge's constant and N the number of carriers.

I.3.c. Detectivity

Detectivity gives a crucial information on the signal-to-noise ration through the Noise Equivalent Power NEP). The NEP is defined as the power of the incident signal for which $\frac{S}{N}$ is equal to 1.

$$D^* = \frac{1}{NEP} = \frac{R \times \sqrt{A}}{N} \; [cm.Hz^{0.5}.W^{-1}]$$

Where A is the area of the detector.

I.3.d. NETD

The Noise Equivalent Differential Temperature is defined as the smallest difference in temperature resolved by a detector, i.e. temperature difference for which the signal is equal to the noise. It depends on external cell parameters such as the reading circuit, the consistency of a matrix of sensors, or even numerical aperture.

I.3.e. Operating temperature

The operating temperature has an implicit impact with parameters defined previously. The increase in temperature leads to a decline in the response of the detector: thermal noise is enhanced and force the electrons to move on excited energy levels which are standing up against photocurrent. As a consequence electron path is less unidirectional. On the other hand, the reduction of power consumption with increasing temperature gives rise to a trade-off temperature.

Chapter II:

Characterization of QCDs and their application for infrared spectroscopy

This section reveals the various physical measures carried out on two samples of QCDs provided by the III-V lab. The first one is sensitive to wavelength equal to 5 µm, and the other one to wavelength equal to 8 µm. A large number of characterization measurements were performed and I am only showing in this report the most important results.

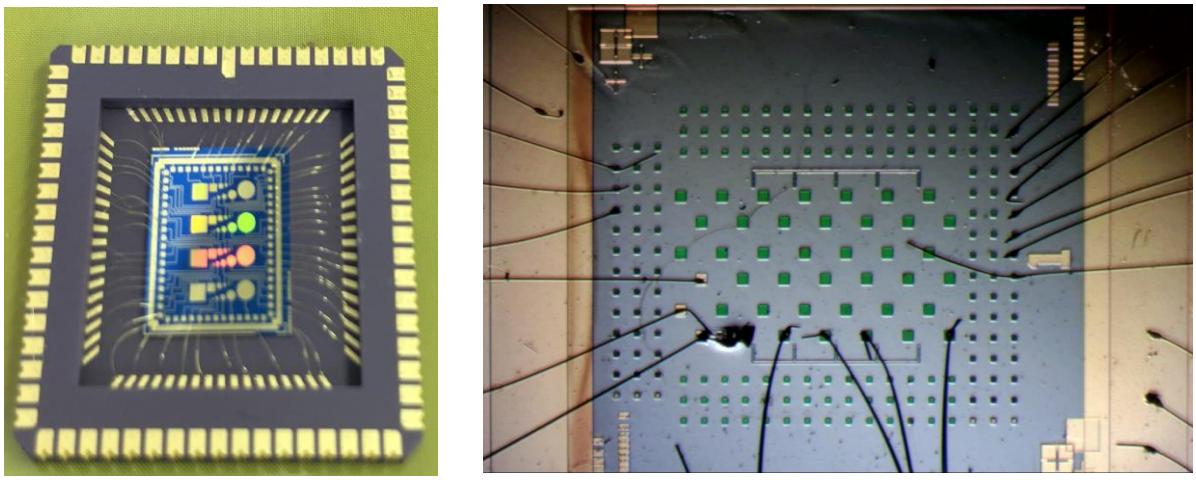

Figure 14: Photos of the two samples of QCDs. To the left: QCDs at 5µm of different geometry and size. To the right, QCDs at 8µm with only two different sizes.

As explained in the introduction, the aim is firstly to observe the physical behaviour of a couple QCL/QCD [9], [10] and then to assess the feasibility of an infrared spectroscopy measurement of this system.

My experimental measurements took place in two stages:

- The characterization of both samples in order to understand their operation as well as the influence of the design on the performances.
- The implementation of an optical bench to perform the spectroscopy of water in the air in order to verify the QCD integration with the MultiSense electronics developed by MirSense.

II.1. Experimental characterization of QCDs

II.1.a. I-V Curves

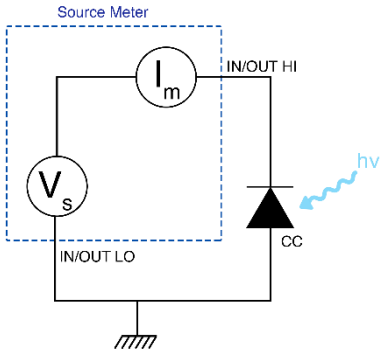

Figure 15: Schematic I-V curves measurement circuit.

The behaviour of the QCD is defined by its characteristic current-voltage (I=f(V)). A source meter Keithley allows to apply a voltage to the terminals of the QCD and quantify the current flowing through this dipole. A low noise source is required to perfom these experiments because of the low level of current provided by the QCD.

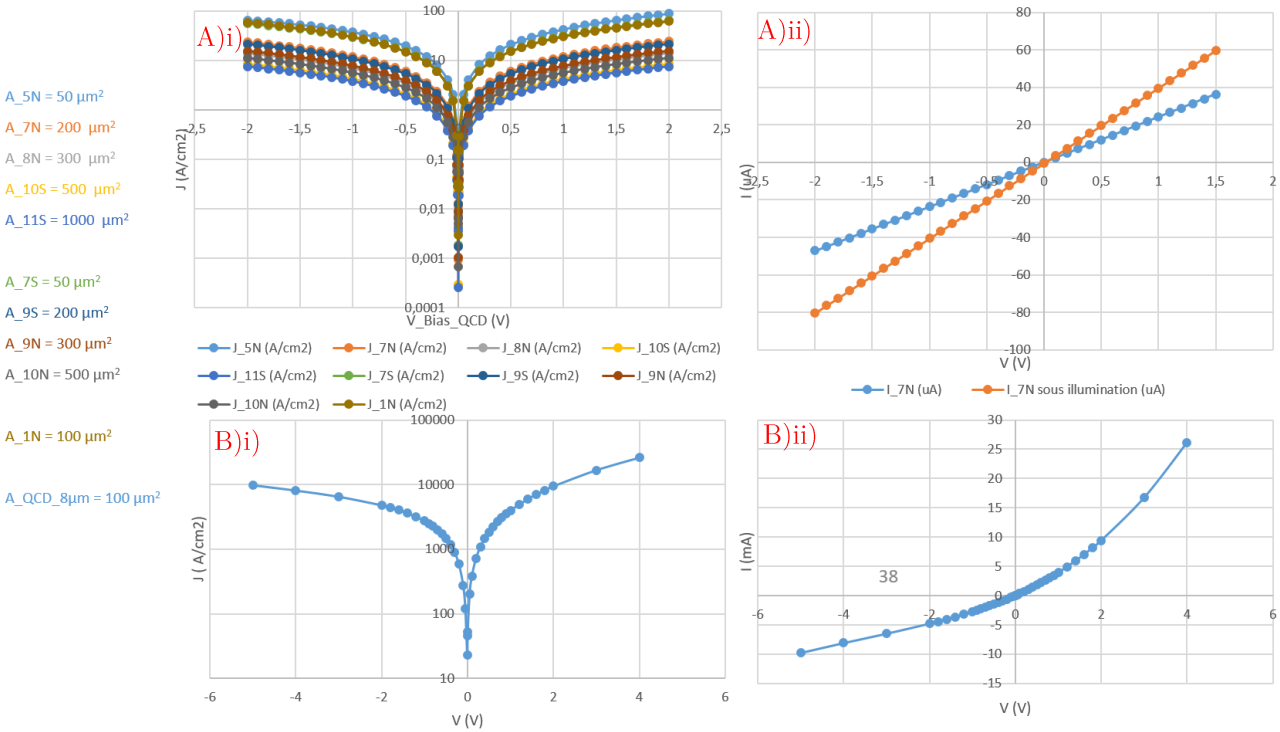

Figure 16: A) Experimental IV curves of QCDs at 5µm i) current density according to the applied voltage and the area in dark condition. ii) I-V curves under illumination and without illumination.

B) Experimental IV curves of QCDs at 8µm i) current density according to the applied voltage in dark condition ii) IV curve without illumination.

The resulting I-V curves are not straight and show the non-linear behaviour of the QCDs. Diode rectifier character is observed and can be expressed as:

$$I_0\left(e^{\frac{\alpha qV}{kT}} - e^{\frac{\beta qV}{kT}}\right) avec\ \alpha \neq \beta$$

The current flowing into the QCD remains more or less constant when the latter is polarized negatively. In this case, the distance between the two levels of the cascade is increased and the electronic transitions that required the lowest energy is the one allowing the transfer of the electron to the following period of the cascade.

Unlike the negative bias, a positive bias reduces the distance between two energy levels of the cascade and prevents the electrons to escape and create a photocurrent.

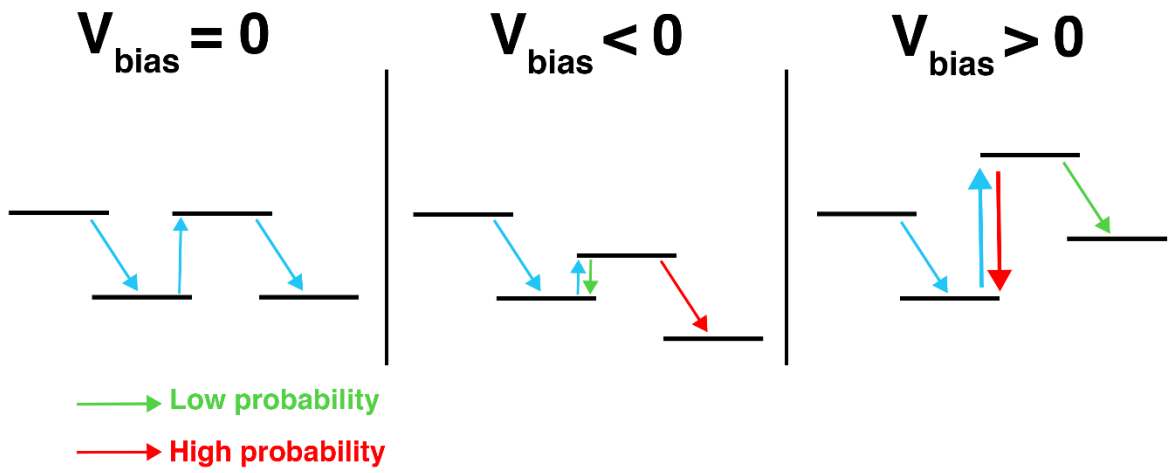

Figure 17: Schematic figure of the different levels of the cascade without and under bias.

These behaviours are verified by the observation of the amplitude of the QCD signal depending of the applied bias represented in figure 17. This curve is obtained by illuminating, thanks to QCL, a QCD bias by a source meter. The peak intensity is reported thanks to an oscilloscope. As we can see from the chart, for a positive bias the signal is lower which testifies a lower photocurrent. As a result, it can be interesting to polarize the QCD with negative bias in order to have higher response. However this benefit has to be balanced by an increase of noise level. Thus a trade-off has to be taken into account in order to find the best signal.

Furthermore, this experience had cautioned us with regard to the sensitivity of QCDs when a high positive bias is applied: their resistance is lower as a result of the diffusion of the contacts into the semiconductor GaAs layer, and thus, the QCD response is drastically reduced.

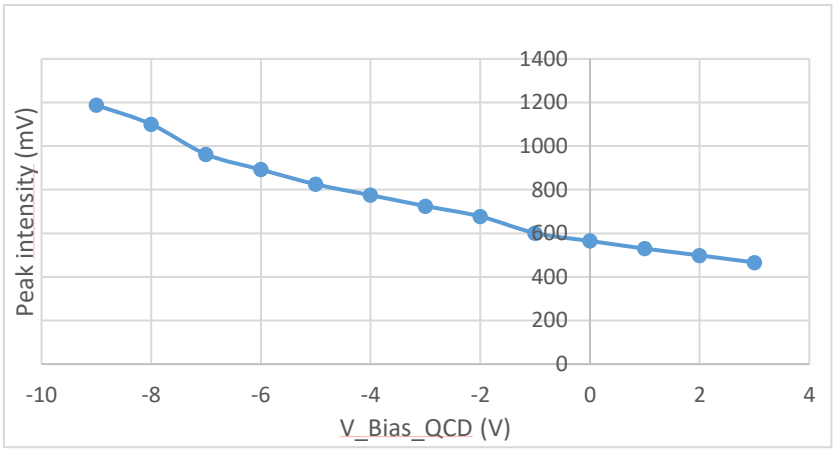

Figure 18: Experimental peak intensity of a QCD at 5µm regarding the bias applied.

II.1.b. Detectivity

In order to study the effect of noise on the detectors, we extracted the value of resistance of the non-polarized QCDs multiplied by their area. This value is linked to the Johnson noise which is dominant in the QCDs: the higher is $R_0 * A$, the lower is the Johnson noise, as supports the figure 18. QCDs at 8µm exhibit in general a noisier signal than QCDs at 5µm and shows a lower response because of their lower absorption energy.

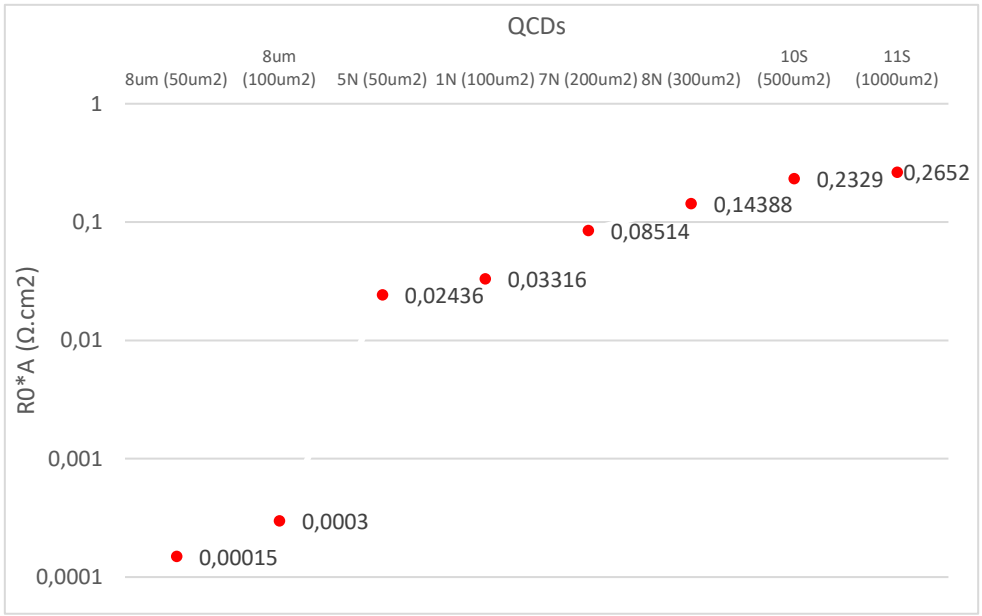

*Figure 19: Experimental results of R0*A for the different QCDs.*

The QCD's detectivity characterizes a detector with respect to its noise. It gives an idea of this ability to detect weak signal. It can be approximated by the following formulas [8]:

$$D^* = \frac{R * \sqrt{A}}{N} where\ N = \sqrt{\frac{4 * kT}{R_0}}\ \ and\ \ R = \frac{\lambda * q * \eta * p_e}{h * c * N_p}$$

Where η is the quantum efficiency, p_e is the extraction probability and, N_p is the number of periods of the cascading structure.

The Numerical application presented here is based on several approximations:

- p_e is set to 0.7 which is the value found in different scientific articles and thesis[8];
- η is approximated to 0.1 since the quantum efficiency of QCDs is smaller than quantum efficiency of QWIP which is of the order of 0.1[8] ;
- N_p à 10, the value provided by the III-V lab. Responsivity is one of the weaknesses of QCDs (28mA/W at 5µm and 45mA/W at 8µm). For this reason the number of periods has to be reduced as much as possible.

The order of magnitude for the detectivity of our QCDs is approximatively:

$$D^*_{5um} = 6 * 10^7\ Jones\ and\ D^*_{8um} = 6 * 10^6\ Jones$$

It is approximatively the same order of magnitude than the values of detectivity of the MCT (10^7 to 10^8 for a detector without cooling and quite fast[1]). However QCD's detectivity can reach the order of magnitude 10^{10} for temperature lower than 80 K [8]. Regarding QWIP, performance comparable in terms of detectivity; even through the quantum efficiency is greater among the QWIP, the response and noise of QCDs are lower.

II.1.c. Responsivity

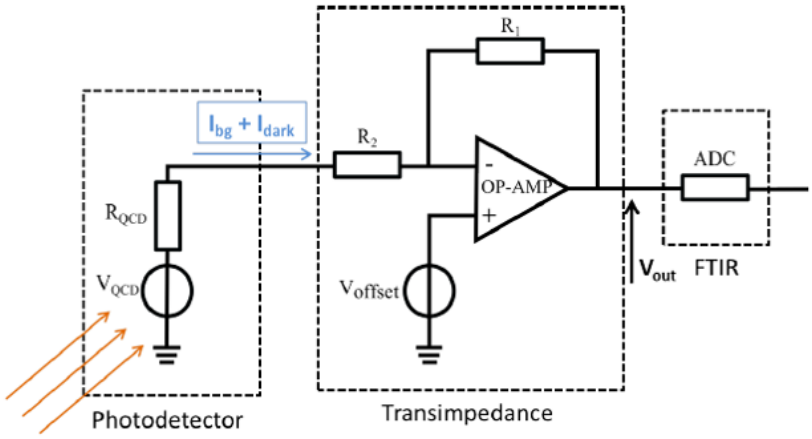

Figure 20: Schematic circuit for the measurement of the QCD's response. [4]

[1] Order of magnitude given by Vigo website

This part is analysing the signal obtained by different QCDs.
A QCL is biased by a pulse generator so as to get a duty cycle of 3% in order to not damage the source. Beyond a certain threshold voltage, the QCL starts to emit light. The light beam passes through a collimation lens and is then focused by a convergent lens on the detector of interest. The light power received by the detector is transformed into a current which is then sent in a Transimpedance Amplifier (TIA) in order to convert the photocurrent generate by the QCD in a voltage (It should be noted that TIA is rapidly overload by weak input impedance of QCDs. Measures at low temperature would be easier and cleaner than those at room temperature). The output voltage is therefore sent on an oscilloscope or a Fourier Transform Infrared Spectroscopy (FTIR) so as to raise the intensity of the signal coming from the QCD for different QCL.
A FTIR includes a Michelson interferometer which is composed of two mirrors, one fixed and the other mobile, and a separator. It is used in order to induce a difference of optical path between two beams. Both lights beams are then recombined and transmitted to a detector that measures the intensity of the signal received according to the optical path difference. As the mobile mirror is subject to a back and forth movement, the intensity of the signal switches between a maximum (constructive interferences) and a minimum (destructive interferences) which gives rise to a sinusoidal signal. A spectrum is then obtained thanks to a Fourier transformed operation.

Different characteristics can be deduced from the result obtained:

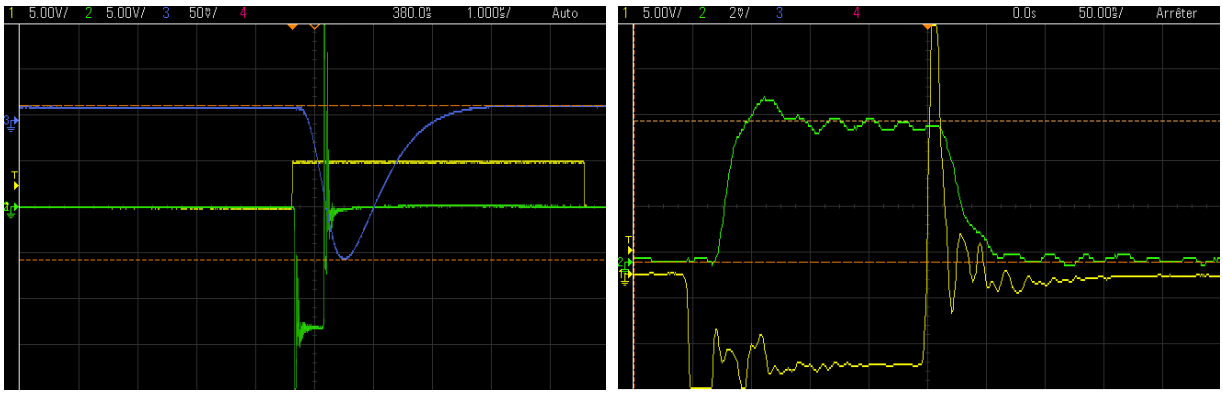

Figure 21: Signal observed at the oscilloscope. To the left: yellow: trigger, green: QCL pulse; blue: QCD response with TIA. To the right: yellow: QCL pulse, green: QCD's response without TIA.

- The first thing to be noticed is the ability to detect QCL signal with our QCDs at room temperature. It is not an ordinary fact because the majority of quantum detectors such as MCT and QWIP has to be cool down to detect a signal. Figure 20 shows the amplitude of the signal coming from the QCD. Direct reading of the signal (i.e. without TIA) gives an idea of the speed of QCDs which is remarkably fast at first sight (of the order of a few nanoseconds). The literature supports our result by attesting that one of the main advantages of QCD consists on an impressive detection speed [11] compared to other detectors such as MCT detectors.

QCDs at 5µm have a smaller responsivity (which is proportional to the wavelength) than those at 8µm, so we had to use a TIA in order to visualize the signal. The pulse deformation observed when using the TIA is due to the cutoff frequency of the TIA.

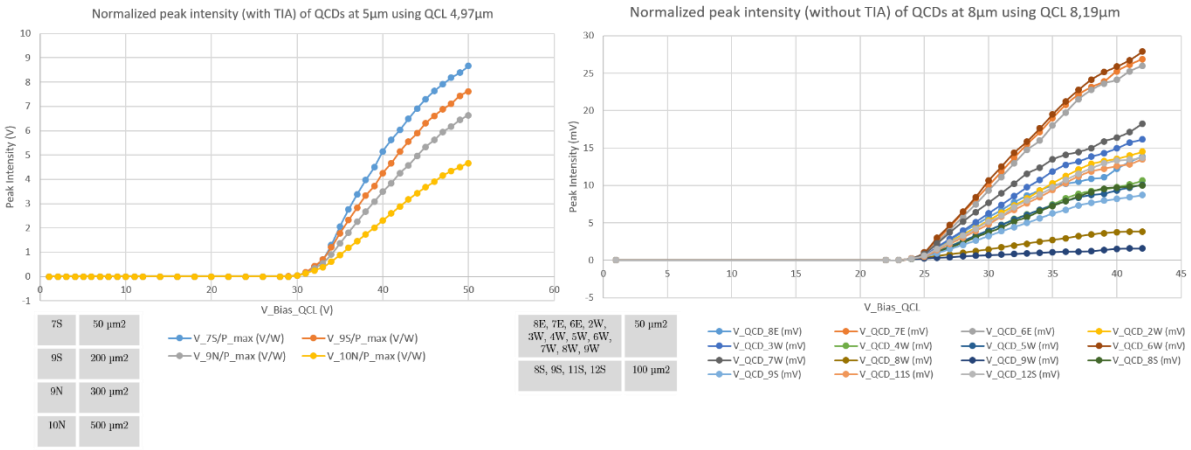

Figure 22: Peak intensities according to the QCL voltage bias raise from oscilloscope.

- The QCD's area does not influence the response of the signal. The signal peak difference seen in the figure 21 comes from an inhomogeneous illumination of the QCD. Indeed when the QCD's area is greater than the area of the beam spot, the observed signal is given by the average current received. However the area plays a crucial role in the minimization of noise. A smaller design is preferred to overcome the noise. Besides QCDs at 8µm show a higher response than those at 5µm contrary to what was predicted in the previous section. This, mainly, comes from the quality of the grating and band structure which were better fabricate in clean room. A Scanning Electron Microscopy (SEM) was performed on the QCDs at 5µm in order to ascertain this last assumption.

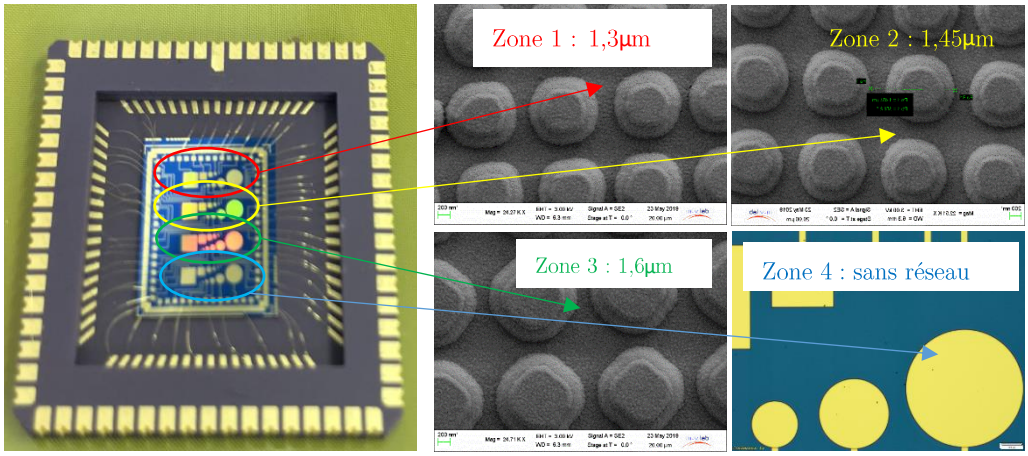

Figure 23: SEM of QCDs at 5µm. They show rounded grating instead of sharp squares.

- As explained previously, gratings [12] have a crucial influence on the QCD's response. Indeed quantum well detectors are sensitive only to a single polarization and a metallic grating is needed to allow the incident light to be absorbed by the active layer. Regarding QCDs at 5 µm, three different grating have been defined as well as an area without grating. The different results obtained in the figure 23 to the left, do no show outrageous difference. It is due, as say previously, to the clean room manufacturing stage during which defects have prevented the fabrication of suitable gratings. On the other hand, the intensity-wavelength curve verifies that the wavelength is shifted to a higher value (in µm) when the grating step is growing. Regarding QCDs at 8 µm which in turn, have much more pure grating, give better signal for QCDs involving a grating and almost zero intensity for QCDs without grating.

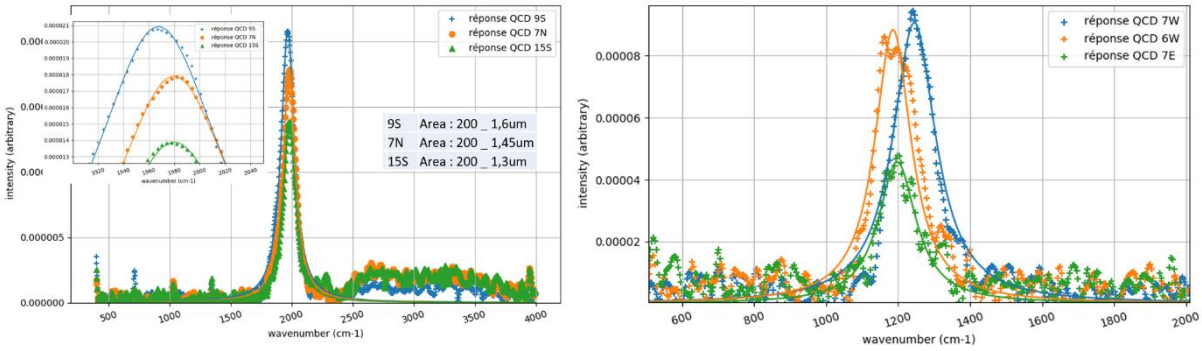

Figure 24: Spectre obtained by the FTIR for QCDs at 5 um to the left and QCDs at 8 um to the right.

- The figures 23 shows the QCD's response. The latter is defined as a convolution of the QCD's gain with the grating etch at the QCD's surface. These curves are also testifying to the spectral bandwidth of QCDs which is of the order of 0.5 µm (FWHM). It is a property welcomed in spectroscopy especially when two absorption lines are relatively closed.

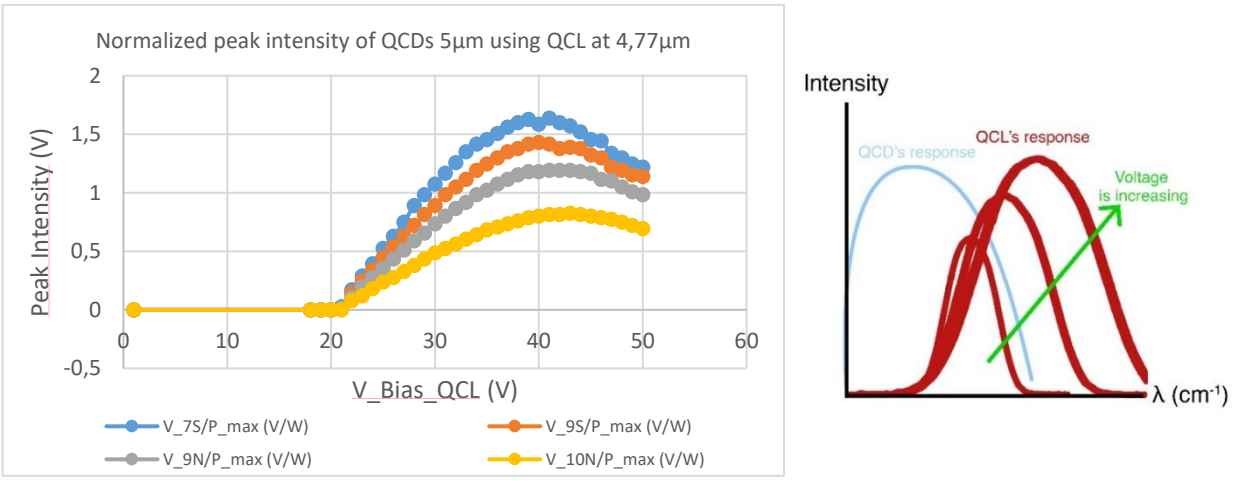

Figure 25: To the left: peak intensities varying with the voltage applied to the QCL. To the right: effect of the voltage applied to the QCL on its spectrum.

- When changing the QCL [13] (increasing or decreasing the wavelength), an unusual curve is obtained. The figure 24 shows a peak for an applied voltage of 40 V. This phenomenon is due to a shift to higher wavelength when the voltage applied is increased. The QCL's response is not anymore matching with the QCD's response which induced a decrease of the intensity at higher voltage.

II.1.d. Noise

The objective of this section consists in an estimation of the noise induced by the detector. This value is a crucial data because signals which have a level below the noise floor will be not observed.

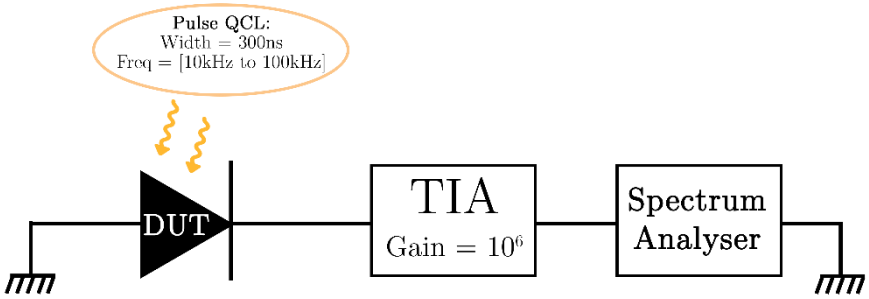

Figure 26: Schematic circuit for noise measurement.

This experiment was performed at the III-V Lab. The QCD is amplified by a TIA and then send on a spectrum analyser in order to observe the Fourier spectrum at the output of the TIA. It is important to note that the measures were carried out by eyes reading and not extracted from a Matlab code (due to computing problems), as we usually do, and so the results will all be given as an order of magnitude.

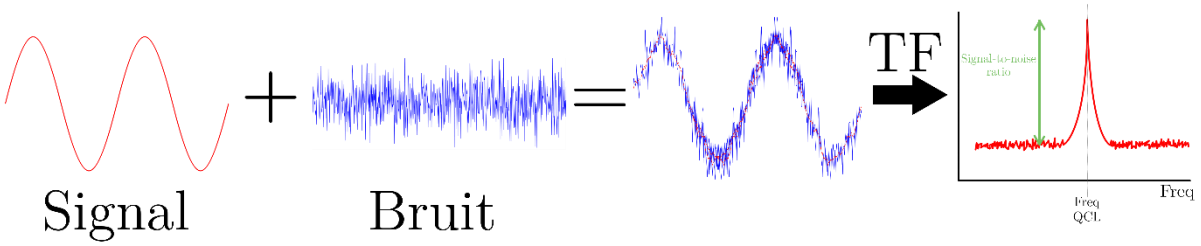

Figure 27: Schematic principle of signal-to-noise measurement.

The noise can be defined from the noise spectral density (NSD) by:

$$N = \sqrt{\int_{f_{min}}^{f_{max}} NSD^2 * df} = NSD * \Delta f$$

Where $\Delta f = \frac{1.22}{2\pi * \tau}$ for a Butterworth filter of order 2 and τ is the integration time equal to 0.5s in our case.

Frist the experiment was performed without QCL light focused on the QCD. The curve obtained constitutes the noise floor. This value is crucial since it represents the noise spectral density required to calculate the noise value.

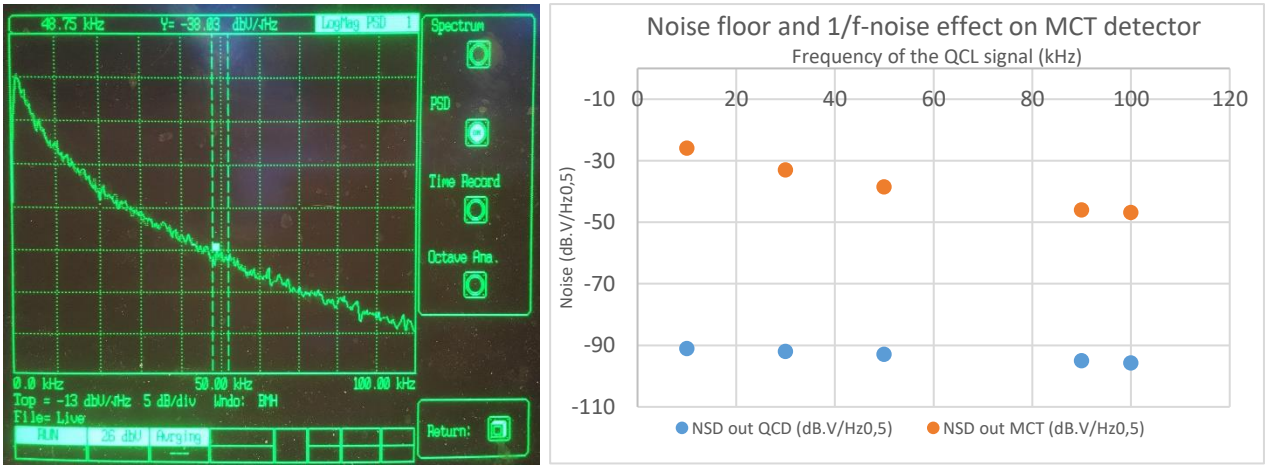

Figure 28: At left: Photo of the MCT's noise floor obtained on the spectrum analyser. At right: Experimental result of the difference of noise floor between a MCT and a QCD.

The figure 28 shows the noise floor for two different detectors. As expected the noise of a QCD does not depend on the frequency. It is called a white noise. Indeed in the first part of this report, noise in QCD is ruled by Johnson noise, the thermal noise which is a white noise. On the contrary, MCT presents a non-negligible 1/f-noise as we can see on the photo.

To obtained noise values, we have to take into account the noise induced by the TIA. The manufacturer's manual informs an equivalent input noise in current of 130 $fA/Hz^{0.5}$ for a gain of 10^6 which is quite low. Thus the NSD has to be converted from $dB.V/Hz^{0.5}$ in $V/Hz^{0.5}$, then divided by the gain in order to obtain a noise value of $A/Hz^{0.5}$ from which we deduced the equivalent input noise of the TIA. Therefore, the order of magnitude obtained for the noise is:

$$N = 2.5 \times 10^{-11} \left[\frac{A}{\sqrt{Hz}}\right] for\ a\ QCD\ and\ 4 \times 10^{-9} \left[\frac{A}{\sqrt{Hz}}\right]\ for\ a\ MCT\ at\ 100kHz$$

Two order of magnitude separate QCD noise value from the MCT noise value. It is coherent because MCT detector noise includes 1/f noise due to current noise which dominates at low frequency, generation-recombination noise which is dominant at higher frequencies, thermal noise, as well as background radiation fluctuations [18].

Regarding QCD value, it is quite hard to compare with exciting studies. Indeed noise measurements in scientific reports are performed on QWIP rather than QCD and in different temperature conditions, the same wavelength of study or the same bias conditions. For example, a QWIP at 8.5µm, at 100K and without bias, has a noise of 1×10^{-15} $[A/\sqrt{Hz}]$ (See Alexandre Delga PhD report [8]). It is delicate to extrapolate results at 300K since the noise is not depending linearly of the temperature; nevertheless

the noise is increased with temperature and it is not fully incorrect to think that the noise order of magnitude of QWIP and QCD is relatively closed. However it is not relevant to use QWIP without bias and noise value is increasing rapidly when this structure is polarized. For this reason, it is interesting to use QCDs which are less subject to noise issues since they can be used without bias.

The second experimental results were obtained under illumination. The QCL signal is focused on the detector and introduces peaks at each multiple of the frequency of the QCL.

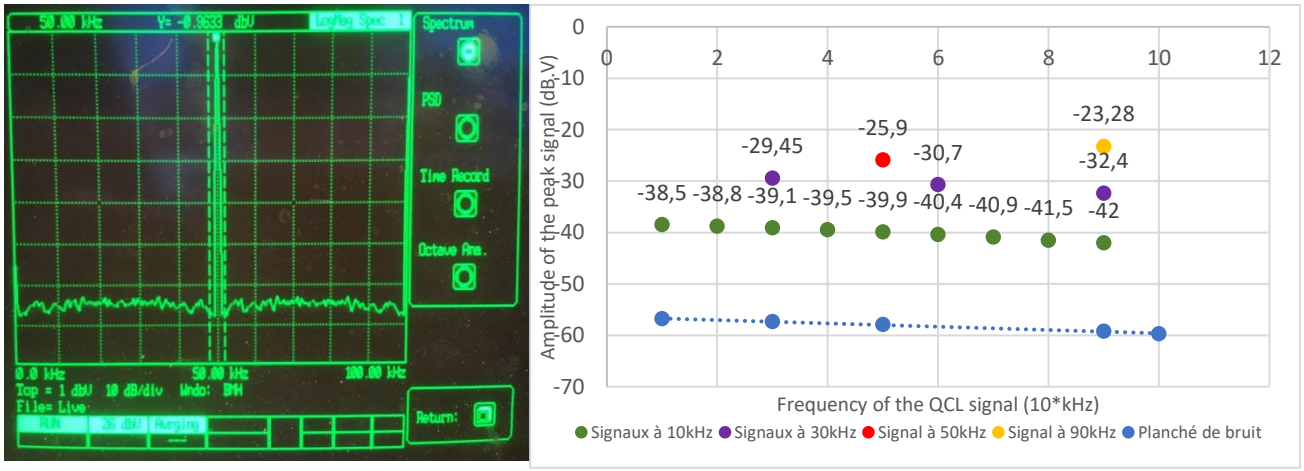

Figure 29: Photo of the Signal observed on the spectral analyser with an MCT. At right: Experimental values of amplitude of the peak signal observed with QCD for different QCL frequencies regarding the noise floor.

The amplitude of the peak in dB.V is converted in V and then divided by the gain in order to find the signal in A of the order of:

$$S = 1 \times 10^{-8}\ [A]\ for\ a\ QCD$$

As expected, this value is quite low and constitute one of the main disadvantages of QCD. Noise is controlled by the fluctuations of electrons between the excited level and the lower level. At high temperature, the number of electrons on the excited level is high and thus the flux of electrons between the lower and higher levels is high. At low temperature the majority of electrons is in the lower level and can hardly access to the higher level. However electrons from the higher level can easily flow to the lowest level. Thus the fluctuations are reduced and the noise is lower. Therefore, contrary to noise which can be improved by a lower temperature, signal (linked to the probability of an electron to escape and produce a current) is lowly dependent on temperature, and becomes a major issue for detectors.

We did not manage to do measurement with the MCT detector since it saturates rapidly. Unlike MCT, QCD are not saturating which allows to have a good signal-to-noise ratio

although the noise level is really high. We calculate the signal-to-noise ratio for our QCD at zero bias and at room temperature:

$$\frac{S}{N} = \frac{1 * 10^{-8}}{2.5 * 10^{-11} * \sqrt{\Delta f}} = 642$$

This value can be overcome by a QWIP with an optimal structure at low temperature for which the value of signal-to-noise ratio is of the order of 7000 [19]. However for a detector that work without bias and at room temperature, the QCD is a suitable choice with a pretty good signal-to-noise ratio and which do not saturate.

II.2. Infrared spectroscopy of water absorption line at 1272cm^{-1}

II.2.a. Setup of the optical bench

Currently, MirSense's laboratory lacks infrastructure allowing the use of unsafe gases. So we decided to focus on gases in ambient air for our spectroscopy experiments. We had to choose: study the water absorption line at 5 µm or the one at 8 µm. Indeed the other gases in the air either own absorption lines that are undetectable by our QCDs either are existing in too small quantity to carry out their spectroscopy.
Then the choice of QCL had set the wavelength of interest. It is essential to choose a QCL whose wavelength lies close to the water absorption line (at more or less 4cm^{-1}), in such a way by changing the surrounding temperature the wavelength shift[14] to the water absorption line. Indeed by increasing the temperature of 10 °C, the wavelength decreases by 1 cm^{-1}. Given the QCL stock of MirSense, we focused on an absorption line at 8 µm. The more intense water absorption line is located at 1272cm^{-1}, so we chose a QCL with wavelength at 1274.472 cm^{-1}.

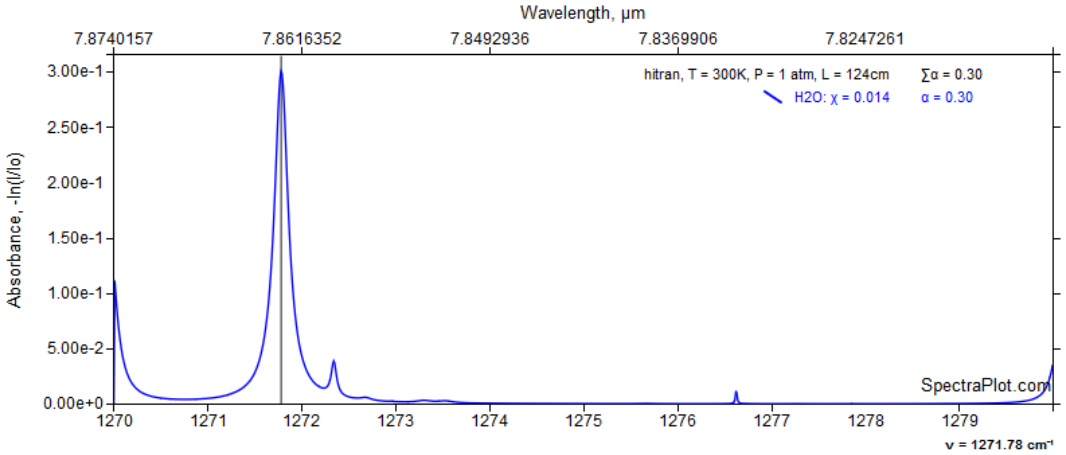

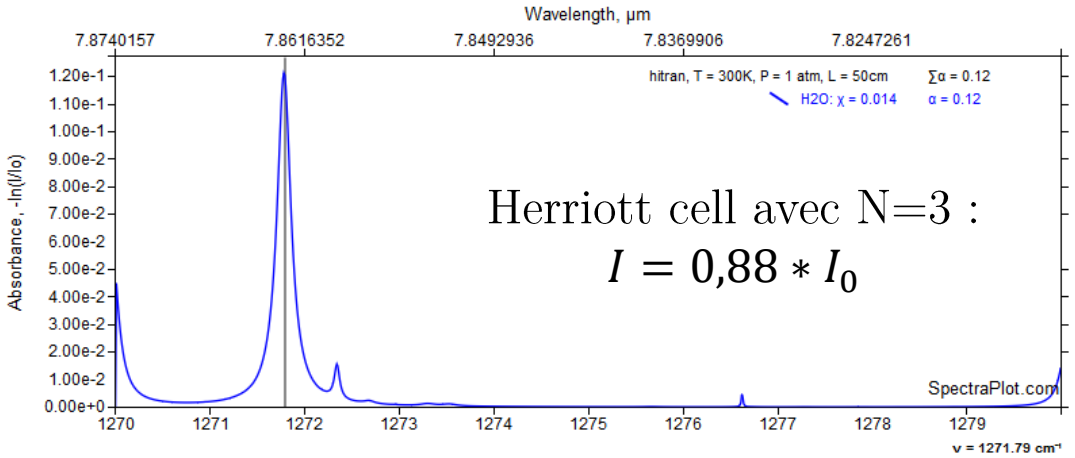

Figure 30: Simulation of absorbance of the water absorption line for two different optical path. (Curves extracted from SpectraPlot Website)

The second step was to ensure the feasibility of the experience for a concentration of water set by the dew point temperature. Knowing the later and by humidity calculations we evaluated the mole fraction of water in the air:

$$t_{dew} = 11.6\,°C \;\leftrightarrow\; p_{sat}(t_{dew}) = 13.66\,hPa$$
$$t_{room} = 25\,°C \;\leftrightarrow\; p_{sat}(t) = 31.67\,hPa$$
$$Relative\ Humidity:\ H_r = \frac{p_{sat}(t_{dew})}{p_{sat}(t)} = 43.1\,\%$$
$$x_{H_2O} = \frac{H_r * p_{sat}(t)}{P_{atm}} = 0.014\ which\ corresponds\ to\ 14000\ ppm$$

Using HITRAN simulation, it was quite easy to predict the absorbance given by:

$$\alpha = -\ln\left(\frac{I}{I_0}\right)\ for\ a\ certain\ optical\ path$$

However this value, reported in figure 25, was not comforting since it was too low to observe the absorption line and we had to find a system in order to increase the distance travelled by the light beam: a Herriott cell.

A Herriott cell [15] is a multi-passages cell which allows the beam to undergo several reflections in order to raise the optical path of the order of several meters and thus improve the sensitivity of the absorption spectroscopy experiment. It is composed of two mirrors, M_1 and M_2, concave with a radius of curvature R_1 and R_2. Each mirror is composed of a hole in order to let the light enter and exit the cell. After crossing the first mirror, the light beam bonce several times within the cell and then leave by the Mirror M_2 right after this last have undergone N reflections. The total distance travelled by the beam is then:

$$L = (2 * N - 1) * d$$

Where d is the distance between the two mirrors.

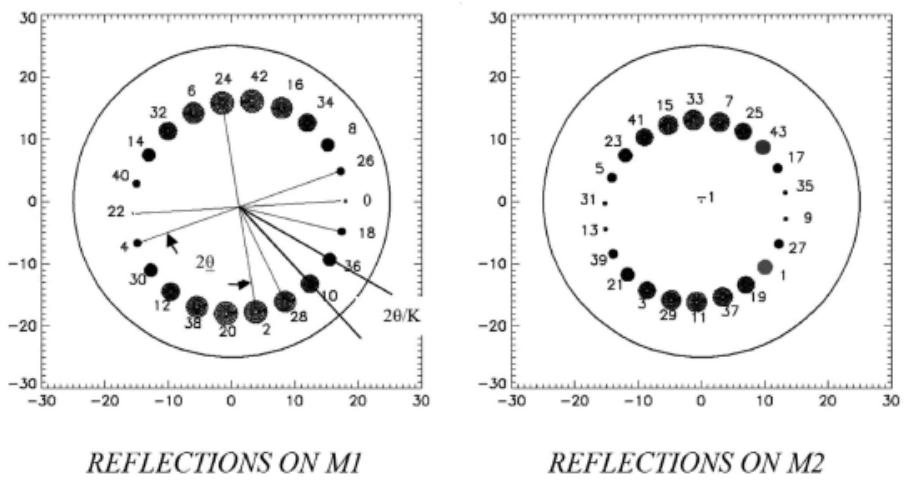

Figure 31: Schematic successive reflections on both mirrors of the cell.

I realized a Pyhton program to adjust the Herriott cell in order to achieve the desired absorption distance. For instance, for N=5 the absorption is equal to α =0.3 and for N=3 it is equal to α =0.12 which correspond respectively of an initial intensity loss of 0.74 and 0.88.

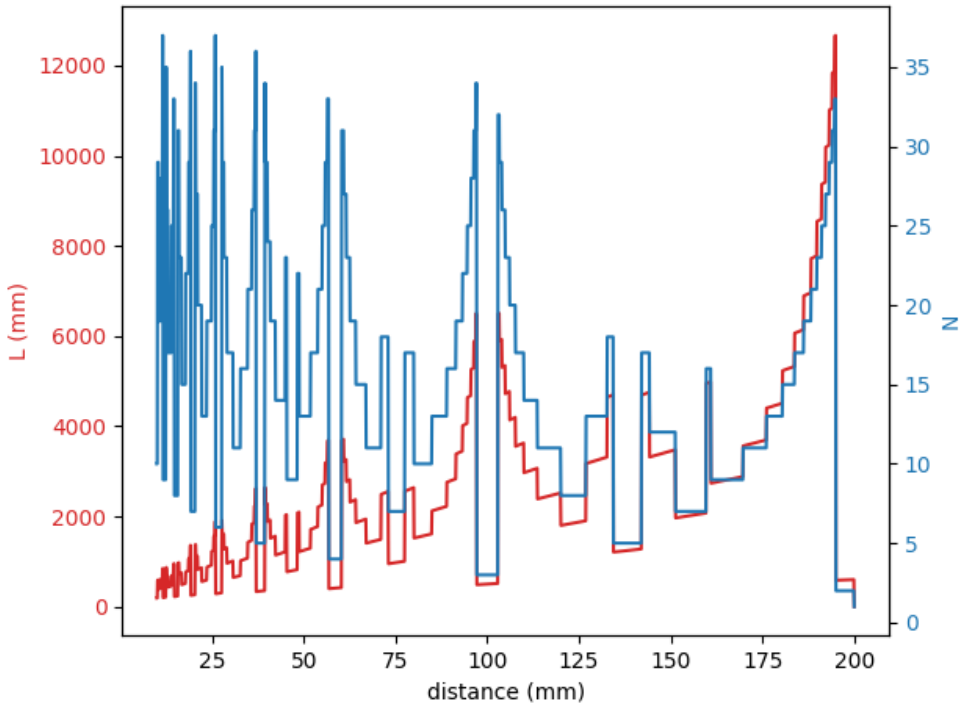

Figure 32: Simulation of the total distance L according to the distance between the mirrors and the number of reflections wanted on the mirror M2.

II.2.b. Measures carried out with MultiSense electronic

Electronics MirSense developed is made for a gas analyser that takes advantage of photoacoustic effect. Here, we are using QCD and no microphone for the detection module.

For our spectroscopy measures it is required to use: a power supply for the QCL source, modulation capabilities, temperature controllers, as well as signal processing capabilities for QCD responses. Therefore to meet these needs, the MultiSense electronic is based on:

- A motherboard which monitors the entire sensor and generate pulses for the QCL;
- Two TECs boards, one is used for the control of the temperature of electronic boards and the other one allows the monitor of the QCL temperature to stabilize the wavelength. Both, electronic and QCL are supported by a Peltier module and thermistor. A water cooling is added to evacuate the heat created at the interfaces;
- A strong signal board to amplify the pulses generated by the motherboard;
- A microphone board linked to the QCD which acts as analog-to-digital converter and includes a lock-in to amplify the signal and remove noise. The lock-in is working only if the incoming signal is modulated at the frequency of a reference signal. The incoming signal is multiplied by the reference signal and then passed in a low pass filter in order to be free of background noise.

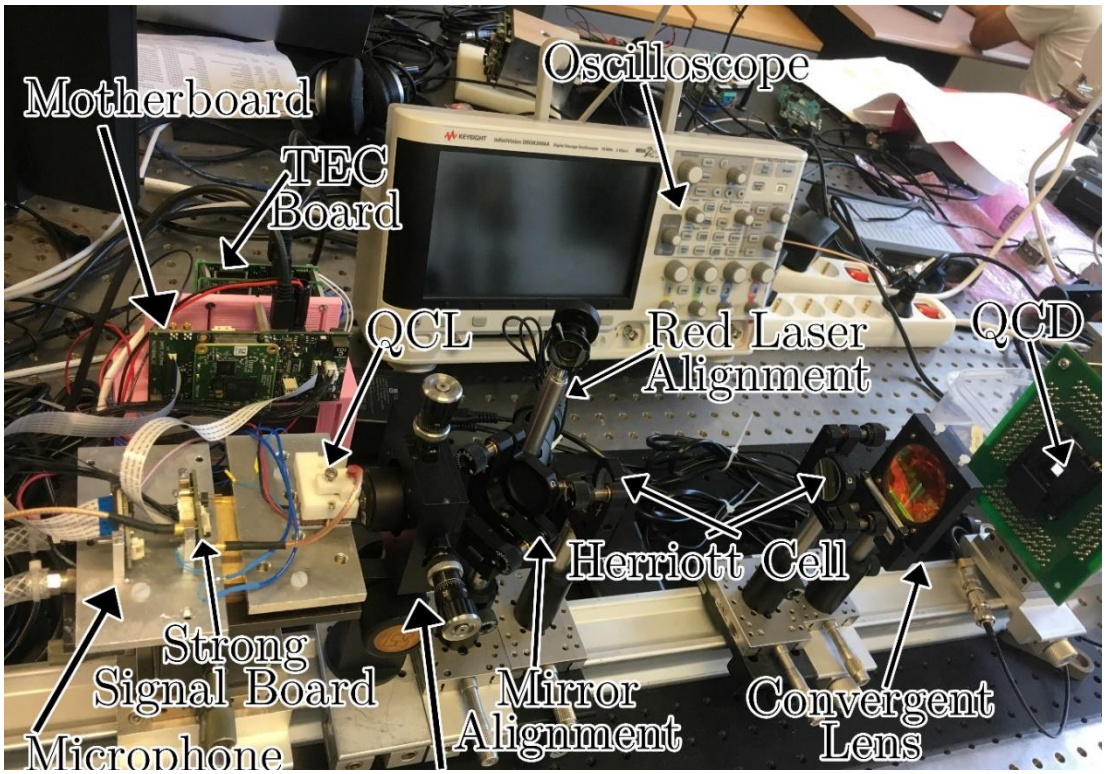

Figure 33: Photo of the optical bench.

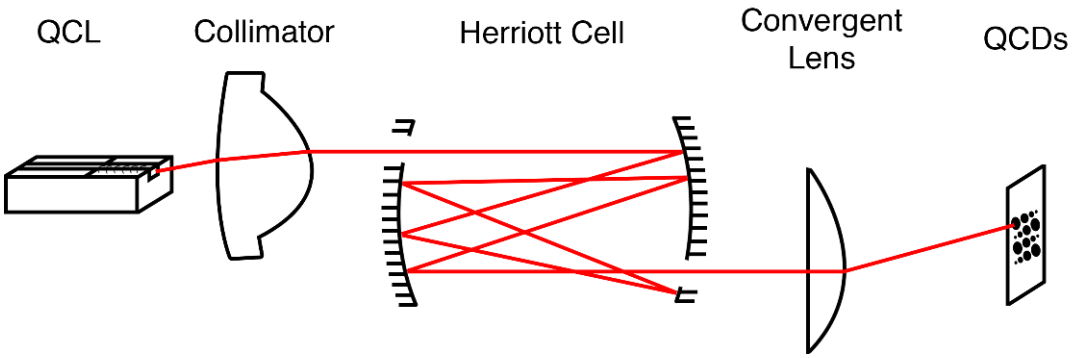

Figure 34: Schematic of the optical bench for gas spectroscopy.[15]

Regarding the optical bench, the QCL emits light and passes through a collimator. Then it reaches the Herriott cell where it bounces several times before exit and be focused by a convergent lens on the detector. First of all we used MCT detector to implement the experience since it is less selective, it will be less restrictive than QCD.

The first step consists in a temperature scan in order to find the position of the absorption line. Then it comes the critical step which is the setting of the modulation parameters. Two modulations are performed: a slow modulation at 0.1 Hz which is a double ramp on a lower current and a modulation at 10 kHz which is a sinus on a lower current. In this way, the slow modulation scans back and forth the absorption line and the sinus modulation scans a small portion of the absorption line which is crucial for a f modulation – f detection approach. Modulation frequencies are chosen in such a way the obtained signal is the fastest and the least noisy as possible.

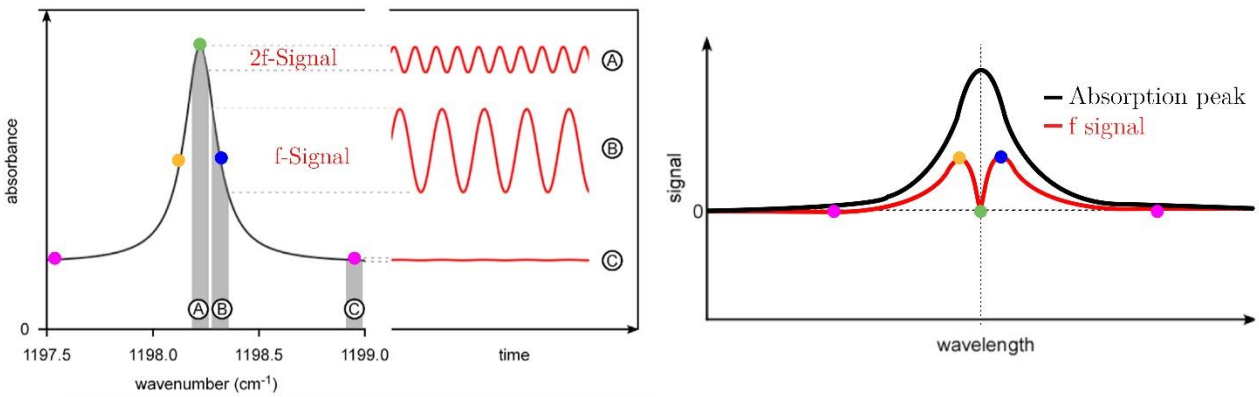

*Figure 35: Schematic absorption peak and the signal observed with an f and 2*f detection approach* [17].

As we can observe in figure 35, the sinus modulation induces a small amplitude signal at frequency 2*f closed to the peak and a high amplitude signal of frequency f where the slope of the curve is the highest. Therefore, the signal obtained for a f detection approach, after being processed the lock-in, is zero for the peak maximum wavelength (A) and at the highest value for both wavelengths of the larger slope curve (B). For

wavelength outside the absorption feature, quasi inexistent amplitude is observed and give a zero signal on the demodulated one.

Regarding the lock-in detection, we applied a Butterworth filter of order two with an integration time of 0.5s. The longer this time, the faithful is the signal; but the slower the integration time, the higher is the noise. This trade-off depends on the scan speed which is the frequency of the slow modulation. Finally we choose to demodulate at the same frequency of the modulation (10 kHz). It is also possible to demodulate at 2*f which eliminate unwanted signals however it is conceptually harder to implement and not relevant in our case since the signal detected is suitable.

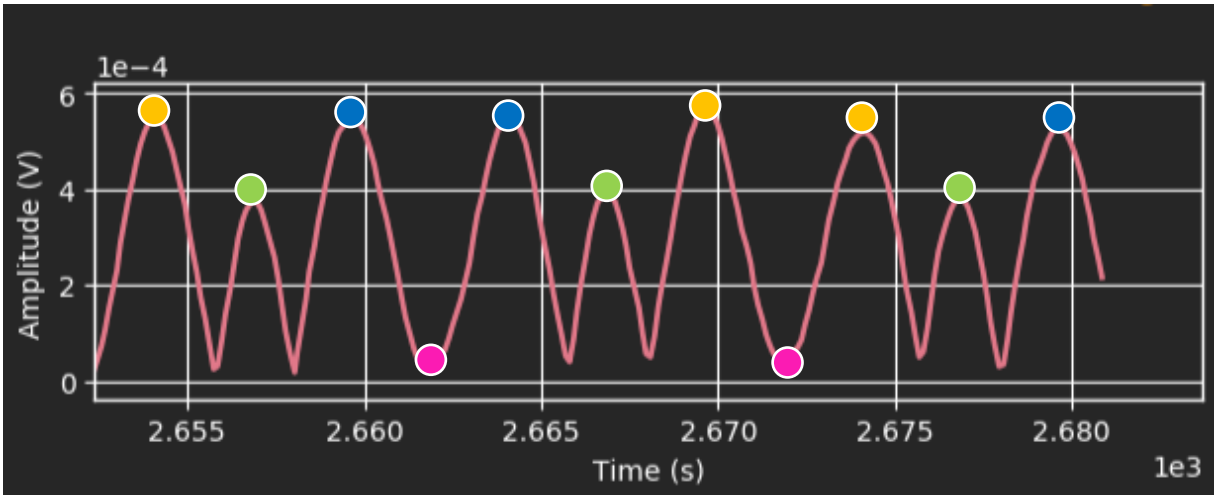

Figure 36: Obtained signal from the MultiSense board with MCT based on the f-f detection method.

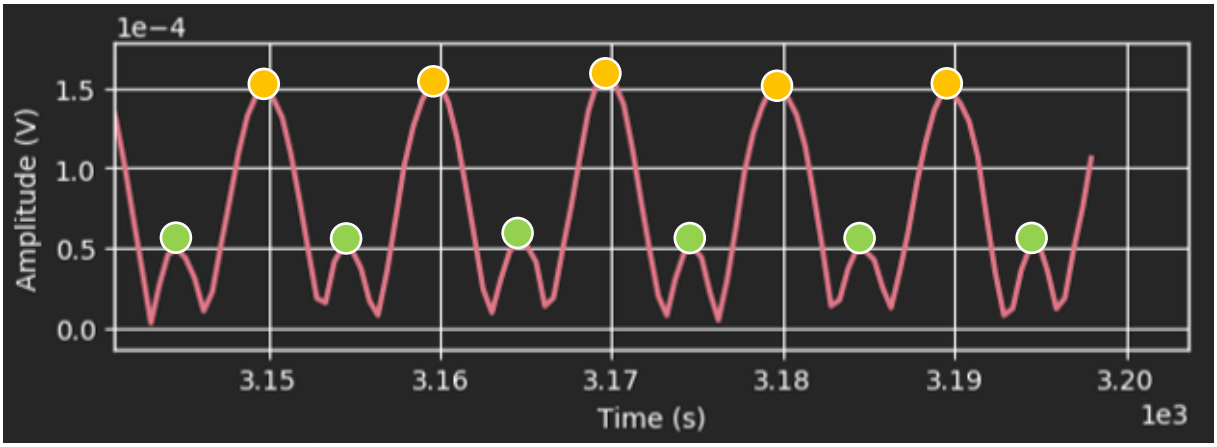

Figure 37: Obtained signal from the MultiSense board with QCD based on the f-f detection method.

The colour circle on the figure 36 and 37 have the same meaning than the colour circle of the figure 35. Green circles represent the absorption peak, pink circles accounts for the wavelength far away from the peak, orange and blue circles depict wavelength centred on the side of the peak.

Firstly, the obtained curves in figure 36 and 37 are not similar to the previous schematic signal demodulated on the right of the figure 35. This difference may come from an offset signal that make slide the origin of the demodulated signal before the lock-in. Indeed, the slow modulation in current send on the source can change the amplitude of the QCL which generate an offset signal, as shown in the figure 38.

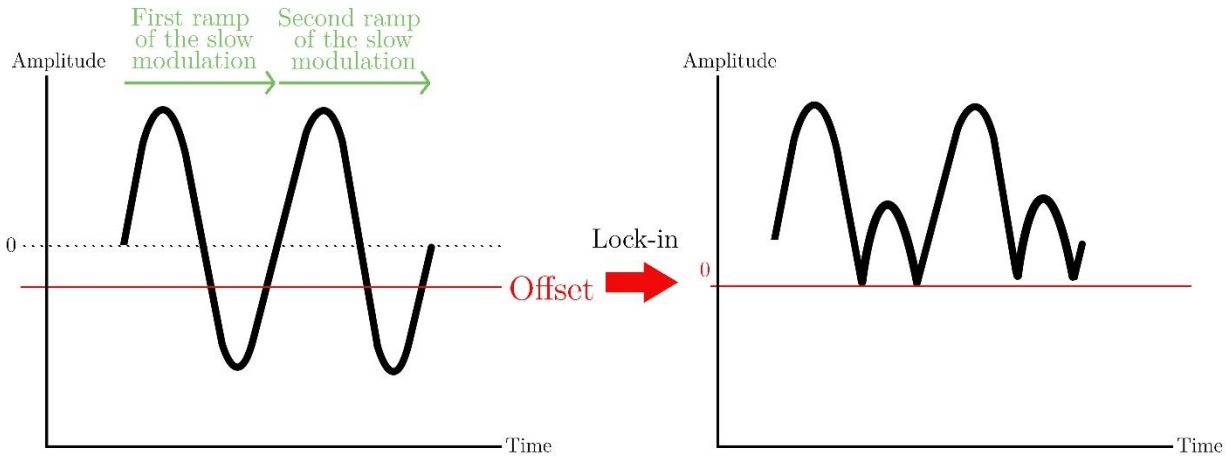

Figure 38: Schematic representation of the effect of an offset on the demodulated signal.

Secondly, curves obtained with the MCT and QCD are not showing the same pattern. I have, on purpose, choose to change the scanning range in temperature. Contrary to the MCT feature that scan the entire absorption peak and below, the curve obtained with the QCD is only showing a part of the absorption peak. Indeed, if the peak was entirely scan, the green circle would be at a higher amplitude. Besides, the absorbance may vary with the time of day (dew point changes), and with the optical alignment.

These results have shown that it was quite difficult to set the right parameters, in particular find the right starting temperature and the modulation parameters, in order to scan the absorption peak. However once the parameters are adjusted, the absorption peak is perfectly observed with the MCT and more importantly with our QCDs. Thus we have demonstrated that it was possible to do gas spectroscopy using Multisense electronic with our QCD.

The signal provided by the electronic MultiSense can be used to extract two main information, which will not be discussed in this report:

- The absorbance which is proportional to the maximum of the curve. From this value and thanks to mathematic tools, we can obtain the water concentration in air.
- The pressure which is linked to the width of the absorption line.

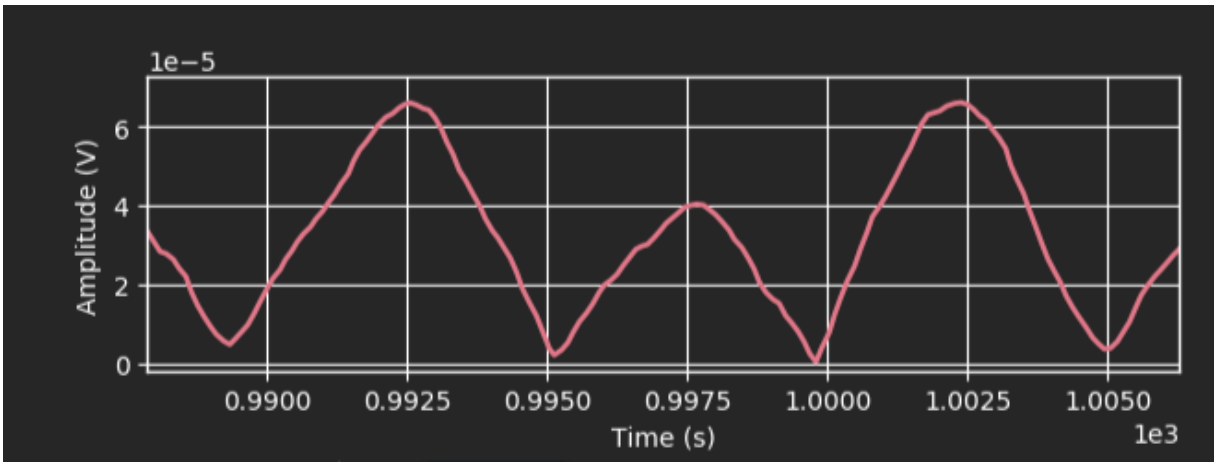

Figure 39: Motif obtained from the MultiSense board with QCD with Herriott Cell set on an absorption distance of 1m23.

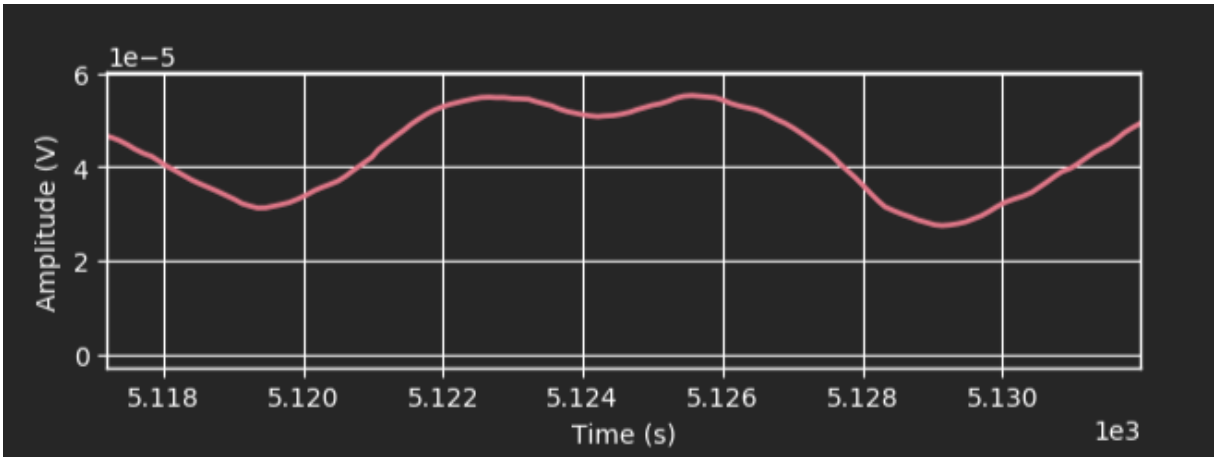

Figure 40: Motif obtained from the MultiSense board with QCD without Herriott Cell.

The last experiment was to prove the necessity of the Herriott cell. I hiked on figure 39 and 40, the demodulation pattern with and without the Herriott cell. As you can see the absorption peak is well defined in the pattern with Herriott cell. However when removing the multi-passages cell, the pattern becomes more or less flat. This phenomenon testifies an absorption too small to be notable. We only see the effect of the offset and temperature. Therefore our estimation was correct, and if we want to integrate in the same chip a QCL and a QCD to perform gas spectroscopy, the optical path will be a crucial issue.

Conclusion:

In the first part of this report, I have highlighted the interest of using QCD for infrared detection. First, as its technology is the same than QCL, an integrated chip with a source laser and QCD detector can be implemented in gas detection modules. However its main interest compared to acoustic detection consists in doing free space communication.

Then, I have presented complete characteristic measurements (I-V curves, response, detectivity and noise) of the quantum cascade detector for which I draw a comparison with MCT and QWIP detectors. The results have shown several benefits of QCD: they are fast, less subject to noise than other detector, and do not saturate. However they are tarnished by a weak response which limits their detectivity some order of magnitude below those of cooled QWIP and MCT.

Finally I verified that QCD can be used with the electronic developed by MirSense and that we are able to do spectroscopy measurement with these detectors. Despite delicate settings that required this experiment, the results were positive and have shown a well-defined absorption peak. However to complete this study I should attract from the results obtained, the water concentration thank to mathematic tools, which required a more precise noise study.

References:

[1] Cédric Koenigner, “Transport électronique dans les détecteurs à cascade quantique”, 2010

[2] Amandine Buffay, “Etude du transport et elaboration de nouveaux détecteurs à cascade quantique pour le lointain infrarouge”, 2011

[3] L. Gendron, “Quantum Cascade detectors”, 2005

[4] Zahra Asghari, “High frequency optoelectronic devices in the mid-infrared wavelength region”

[5] H.C. Liu, Frederico Capasso, “Intersubband transitions in quantum well : Physics and device applications II”, Semiconductors and semimetals volume 62

[6] Gregory Maisons, “Réalisation de sources laser monomodes innovantes émettant dans le moyen infrarouge. Application à la spectroscopie”, 2006

[7] Thomas Antoni, “Structures de couplage optique originales pour les détecteurs infrarouge à puits quantiques”, 2009

[8] Alexandre Delga, “Du phénomène quantique au dispositive macroscopique, transport électronique dans les détecteurs inter-sousbandes”, 2013

[9] Andreas Harrer, “Mid-infrared surface transmitting and detecting quantum cascade device for gas-sensing”, Nature, 2016

[10] Benedikt Schwarz, “Monolithically integrated mid-infrared quantum cascade laser and detector”, Sensors 13, 2013

[11] Marcel Graf, “Design and characterisation of far and mid-infrared quantum cascade detector”, 2006

[12] Clement Gilles, “Optique intégrée pour sources largement accordables moyen-infrarouge”, 2017

[13] Jérôme Faist, “Quantum Cascade Laser”, Oxford

[14] Y. Bai, “Highly temperature sensitive quantum cascade lasers”, Applied Physics letters 97, 2010

[15] Claude Robert, “Simple, stable, and compact multiple-reflection optical cell for very long optical paths”, Applied Optics, 2007

[16] Myriam Raybaut, “Détection d’espèces par spectroscopie photoacoustique : principe et applications”, Photoniques, juillet/aout 2011

[17] Daylight solution, “A brief comparison of 2f and broadly swept detection techniques”, 2007

[18] Hamamatsu Photonics, “Characteristics and use of infrared detectors”, 2011

[19] Alexandru Nedelcu, "Enhanced broadband (11-15 µm) QWIP FPAs for space applications", Proc. SPIE 10566, International Conference on Space Optics — ICSO 2008, 105662T, 2017